



Delft University of Technology

Mathematical model for piled embankments on saturated soft clay

Mangraviti, Viviana; Dijkstra, Jelke; Flessati, Luca; Di Prisco, Claudio

DOI

[10.1680/jgeot.24.01090](https://doi.org/10.1680/jgeot.24.01090)

Publication date

2025

Document Version

Final published version

Published in

Geotechnique

Citation (APA)

Mangraviti, V., Dijkstra, J., Flessati, L., & Di Prisco, C. (2025). Mathematical model for piled embankments on saturated soft clay. *Geotechnique*. <https://doi.org/10.1680/jgeot.24.01090>

Important note

To cite this publication, please use the final published version (if applicable). Please check the document version above.

Copyright

Other than for strictly personal use, it is not permitted to download, forward or distribute the text or part of it, without the consent of the author(s) and/or copyright holder(s), unless the work is under an open content license such as Creative Commons.

Takedown policy

Please contact us and provide details if you believe this document breaches copyrights. We will remove access to the work immediately and investigate your claim.

Mathematical model for piled embankments on saturated soft clay

VIVIANA MANGRAVITI*, JELKE DIJKSTRA†, LUCA FLESSATI‡ and CLAUDIO DI PRISCO§

Piled embankments are traditionally designed by using either guidelines based on simplified limit-equilibrium theories or advanced finite-element (FE) numerical analyses. Both methods have limitations: the former do not allow the assessment of settlements at the top of the embankment, whereas the latter easily become overly complex, hence limiting practical applications. This paper introduces a new mathematical model capable of reproducing, with minimal computational effort, the mechanical response of piled embankments modelled by means of FEs. The model is based on a set of fundamental principles, assumptions and phenomenological equations obtained from a deep understanding of the mechanics behind the FE problem. The model, evaluating average and differential settlements at the top of the embankment during the consolidation of the soft soil, is validated against full-scale test data and benchmarked against independent numerical results. The results are compared with existing formulas to evaluate the critical height of the embankment, demonstrating the great potential of the new model for engineering practice (giving nearly instantaneous displacement-based solutions for the design of piled embankments in a preliminary stage).

KEYWORDS: consolidation; embankments; piled embankment; settlement; theoretical analysis

INTRODUCTION

Piled embankments are very challenging geotechnical systems composed of embankment material, concrete piles and foundation soil. They are widely used to reduce settlements of engineered embankments built on soft soil deposits. The marked difference between the stiffness of concrete piles and surrounding soft soil leads to the development of differential settlements at the base of the embankment. This induces (a) the ‘arching effect’ (Marston, 1913; Terzaghi, 1936; McKelvey, 1994; van Eekelen *et al.*, 2013), that is the transfer of stress within the embankment towards pile heads; (b) localisation of shear strains experimentally observed (Da Silva Burke & Elshafie, 2021) in the ‘process zone’ (di Prisco *et al.*, 2020; Mangraviti *et al.*, 2023a, 2023b), that is a thin plastic subdomain close to the pile edge, propagating upwards from the base of the embankment; and (c) the ‘plane of equal settlements’ (PES) (Terzaghi, 1936; McKelvey, 1994; McGuire, 2011), that is the locus where differential settlements between the region of embankment above piles and the one above foundation soil are negligible. The combination of these three mechanisms is affected by the embankment construction rate (Jenck *et al.*, 2009) and governs the time-dependent mechanical response of the system. However, the embankment construction rate affecting the mechanical response of piled embankments has not yet been investigated. The

redistribution of vertical stresses takes place in general both within the embankment and under the foundation plane owing to the roughness of piles shaft (Combarieu, 1988). In this paper, the authors focus on the mechanisms developing in the embankment, by assuming the pile shaft to be smooth.

The accurate prediction over time of the development of settlements is of paramount importance for the alignment, and hence the proper functioning of line infrastructure built on an embankment. In the last few decades, three-dimensional (3D) numerical studies have been carried out to model piled embankments. The behaviour of piled embankments is time dependent and requires coupled hydraulic and mechanical modelling (Huang & Han, 2010; Rowe & Liu, 2015). Nevertheless, 3D hydromechanical coupled numerical analyses are not very common in design practice, being computationally demanding (Bhasi & Rajagopal, 2015). In many cases, the embankment construction is simulated under drained conditions by disregarding the increase in excess pore pressure in the foundation soil (Jenck *et al.*, 2009). Therefore, for practical reasons, many researchers in the past have successfully modelled axisymmetric unit cells to study the performance of the central part of piled embankments (Han & Akins, 2002; Smith & Filz, 2007; Bhasi & Rajagopal, 2015). However, due to the large stiffness gradient between piles and soil managed by interface elements, when time dependency is accounted for, even simplified calculations are time consuming to run (central processing unit (CPU) run time can vary between 24 and 48 h). To this must be added the time required to set up the finite-element (FE) model, evaluate the effects of mesh size/time step on the numerical results and validate the model against real case studies. These operations may require the involvement of an operator at additional cost.

The most commonly used design approaches are based on simplified models defined in the framework of the limit equilibrium method (BSI, 2010; EBGEO, 2010; van Eekelen & Brugman, 2016), disregarding the stiffness of the elements and not allowing the calculation of the evolution of settlements with time at the top of piled embankments. Only ASIRI (2012) suggests an alternative approach to

Manuscript received 23 April 2024; revised manuscript accepted 4 April 2025.

Published with permission by Emerald Publishing Limited under the CC-BY 4.0 license. (<http://creativecommons.org/licenses/by/4.0/>)

* Department of Civil, Environmental and Architectural Engineering, Università di Padova, Padua, Italy; Department of Architecture and Civil Engineering, Chalmers University of Technology, Gothenburg, Sweden (Orcid:0000-0003-3385-1883).

† Department of Architecture and Civil Engineering, Chalmers University of Technology, Gothenburg, Sweden (Orcid:0000-0003-3792-0727).

‡ Faculty of Civil Engineering and Geosciences, Delft University of Technology, Delft, the Netherlands (Orcid:0000-0002-9586-3057).

§ Department of Civil and Environmental Engineering, Politecnico di Milano, Milan, Italy (Orcid:0000-0002-9245-6587).

calculate settlements and homogenised vertical stress distribution along piles including foundation soil stiffness as input data (Cuira & Simon, 2009).

Guidelines usually assume the displacements at the top of the embankment under serviceability conditions to be always nil except for the case of shallow embankments (SEs), where the final height of the embankment is smaller than a 'critical height'. According to all the standards, the critical height is unique, independently of the construction time. One goal of this paper is to demonstrate the opposite. Furthermore, all the formulas for the critical height in the standards are a function of only geometrical quantities (i.e. pile spacing and diameter) and have been derived from results of trap-door tests. However, in a trap-door test, the influence of evolving subsoil stiffness between columns during consolidation is ignored by assuming a uniform settlement profile. Therefore, the arching stresses calculated using standard design methods at ultimate state differ considerably from each other (Naughton & Kempton, 2005; Pham & Dias, 2021) and from those measured in the field (King *et al.*, 2017; Pham & Dias, 2021). A first step towards linking arching stresses in the embankment with settlements in the foundation soil was made by Iglesia *et al.* (2014) and King *et al.* (2017), who introduced the 'ground reaction curve'. However, this approach does not allow the displacements at the top of the embankment to be calculated.

Both the absence of valid theoretical methods and the excessive time needed to perform numerical analyses make the estimation of settlements at the top of piled embankments very challenging. For this reason, di Prisco *et al.* (2020) proposed a mathematical model capable of satisfactorily reproducing the results obtained for the simulated construction of an embankment founded on end-bearing smooth piles and coarse foundation soil. The model has been extended to the case of rough piles by Flessati *et al.* (2023) and to geosynthetic reinforced and pile-supported embankments by di Prisco *et al.* (2019), Mangraviti *et al.* (2021, 2023b) and Mangraviti (2022). However, all these models do not consider the consolidation process, assuming drained conditions for the subsoil during the embankment construction. The novelty of the current paper concerns the study of stress-transfer mechanisms from the embankment to the piles, in the case of fine-grained materials in the foundation soil, and how these are severely influenced by the consolidation process.

In this paper, a new mathematical model to calculate settlements at the top of piled embankments on soft soil during consolidation is illustrated. The mathematical model proposed in this study is a model of a FE model built to be computationally efficient for use in the preliminary design of the time-dependent response of piled embankments, where

materials with vastly different stiffnesses interact. The mathematical model is based on few hypotheses and equations, and capable of instantaneously (less than a minute) predicting the mechanical response of such a complex geo-structure modelled with computationally demanding FE simulations.

To understand the mechanics behind the problem and the way the embankment construction rate affects the mechanical response of the system, hydro-mechanical coupled non-linear FE analyses (section 'FE numerical results') have been performed looking at the concepts of PES (subsection 'Plane of equal settlements'); process height (subsection 'Process height') and the arching effect (subsection 'Arching effect'). The new mathematical model (illustrated in section 'Mathematical modelling'), including both the cases of 'deep' embankment (DE) and SE, has been calibrated on few numerical simulations (section 'Mathematical model calibration') and benchmarked against independent numerical parametric study (subsection 'Comparison with numerical results'). Furthermore, it was validated against field measurements from a full-scale experiment, other numerical studies from the literature and a centrifuge test (subsection 'Validation on experimental data and other numerical studies'). In the fifth section 'Discussion and comparison with existing formulas', the practical application of the mathematical model is illustrated by discussing and comparing the results in terms of critical height of the embankment against some of the most popular formulas published in the literature and suggested by standards.

FE NUMERICAL RESULTS

The authors have numerically analysed the consolidation process in the foundation soil due to the construction of an h -high piled embankment (Fig. 1(a)) by using Tochnog Professional (2019) FE code under small strains. As the focus was on the settlement response, the mechanical response of an axisymmetric representative unit cell is considered (Fig. 1(b)), where the equivalent diameter, s (calculated as in McGuire (2011)), includes: (a) one pile of diameter d and length l ; (b) a homogeneous clay layer of thickness l ; (c) an embankment of height h ; and (d) a rigid bedrock. Usually, vertical piles are socketed in the rigid stratum, but, for the sake of simplicity, this geometrical aspect is disregarded. A 'fine' mesh is used, consisting of six-noded triangular elements with seven integration points for each element. The number of integration points is the same for both soil and water. The mesh is refined near the pile edge (where the largest strains are expected) up to $0.1d$ and optimised to not affect the numerical results (Mangraviti,

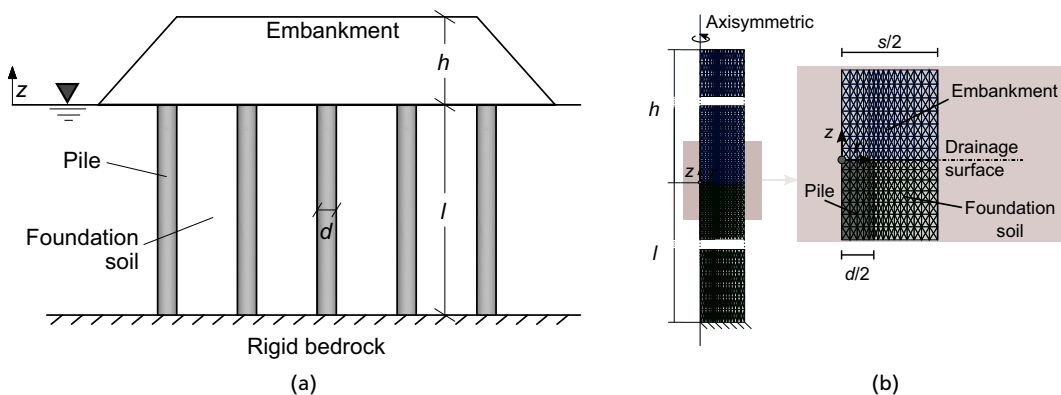


Fig. 1. (a) Piled embankment based on end-bearing piles and saturated soil. (b) Geometry and mesh of the equivalent representative unit cell modelled with finite elements (FE)

2021). Normal displacements are not allowed on both lateral boundaries or at the base.

The construction process is assumed to be instantaneous (i.e. construction rate significantly larger than consolidation rate) and, therefore, for simplicity, in all the simulations, time $t = 0$ refers to the end of the construction phase. Piles are assumed to be smooth and end-bearing. The homogeneous foundation soil is assumed to be saturated and hydraulically isotropic, whereas the water table is assumed to be coincident with the ground level ($z = 0$, where drainage is permitted). The pile, as well as both bottom and lateral boundaries, are assumed to be impervious.

Initial pore pressure before embankment construction was imposed to be hydrostatic since pile installation effects are beyond the scope of this study.

The pile is assumed to behave elastically, whereas, in agreement with other authors (Han *et al.*, 2007; Chen *et al.*, 2008; Huang & Han, 2010; McGuire, 2011; Zheng *et al.*, 2019; Wijerathna & Liyanapathirana, 2020), the mechanical behaviour of the soil within and below the embankment is assumed to be elastic–perfectly plastic, with a Mohr–Coulomb failure criterion and a non-associated flow rule. More sophisticated elastoplastic constitutive relationships for the numerical analysis of similar geometry are employed by Jenck *et al.* (2009), where the response of the unit cell is compared with 3D numerical results. The use of simple elastic–plastic constitutive relationships is justified by their popularity and by the aim of the paper, consisting in introducing the upscaled mathematical model illustrated in the third section ‘Mathematical modelling’. The use of more sophisticated constitutive relationships for FE method analysis would require a slight modification of the laws governing the response of the sub-structures defined in the subsection ‘Sub-structuring approach’, but not a change in the overall mathematical model set-up. Zero-thickness interface elements are introduced between pile and foundation soil. The elastic stiffnesses in normal and tangential directions (4.4×10^5 kN/m³ and 2.2×10^5 kN/m³, respectively) of the no-tension/no-friction interface elements were chosen, in accordance with the software manual (*Tochnog Professional, Version 22* (Tochnog Professional, 2019)), as a function of the neighbouring elements’ stiffness and size.

After rapid construction, the height of the embankment is kept constant and the consolidation is monitored.

The FE numerical analyses have been subdivided into the three following stages.

(a) The state of stress before the embankment construction is initialised for both pile and soft soil by applying gravity under drained conditions and by employing the standard Jaky’s formula.

(b) After the displacements have been reset (settlements due to pile installation effects are not the object of this study), the elements representing the whole embankment are activated very rapidly (30 s) to simulate an ideal undrained embankment construction (i.e. without dissipation in the excess pore water pressure). At the end of this phase, the excess pore water pressure is equal to 99% of γh , where γ is the unit weight of the soil in the embankment.

(c) The problem geometry is kept constant during consolidation.

With the aim of understanding the mechanical response, the numerical results are here discussed for two reference cases, representative for both SE and DE (geometry and mechanical properties in Tables 1 and 2, respectively). The effect of embankment dilatancy angle is included in this study and discussed in subsection ‘Comparison with numerical results’.

Plane of equal settlements

Owing to the model hypotheses, settlements along the radial coordinate, r (Fig. 1(b)), are nearly constant above both concrete pile (subscript c for $0 < r < d/2$) and foundation soil (subscript f for $d/2 < r < s/2$). Consequently, average values can be used to monitor the evolution with time of settlements at both embankment base (u_b) and top (u_t):

$$u_{b,f} = \frac{2\pi \int_{d/2}^{s/2} u(z = 0, r) r dr}{\pi(s^2 - d^2)/4} \quad (1)$$

$$u_{t,av} = \frac{u_{t,f}(s^2 - d^2) + u_{t,c}(d^2)}{s^2} \quad (2)$$

where

$$u_{t,c} = \frac{2\pi \int_0^{d/2} u(z = h, r) r dr}{\pi d^2/4}; \quad u_{t,f} = \frac{2\pi \int_{d/2}^{s/2} u(z = h, r) r dr}{\pi(s^2 - d^2)/4} \quad (3)$$

For the DE case, since the embankment height is larger and the settlements due to the embankment self-weight are included in the calculation, $u_{b,f}$ and $u_{t,av}$ are larger than for the SE case (Figs 2(a) and 2(b)). In contrast, differential settlements at the top:

$$u_{t,diff} = u_{t,f} - u_{t,c} \quad (4)$$

are nil for any t value in the case of DE, whereas they progressively increase with time in the case of SE (Fig. 2(c)). In particular, at the beginning of consolidation, differential

Table 1. Geometry of the reference cases

Reference cases	h : m	d : m	l : m	s : m
Deep embankment (DE)	5	0.5	5	1.5
Shallow embankment (SE)	1	0.5	5	1.5

Table 2. Mechanical and hydraulic properties for the reference cases

	Unit weight: kN/m ³	Young’s modulus: MPa	Friction angle: degrees	Cohesion: kPa	Dilatancy angle: degrees	Hydraulic conductivity: m/s
Soft soil	18	1	30	0	0	4×10^{-9}
Embankment	18	10	40	0	0	1×10^{-3}
Pile	25	30 000	—	—	—	Impervious

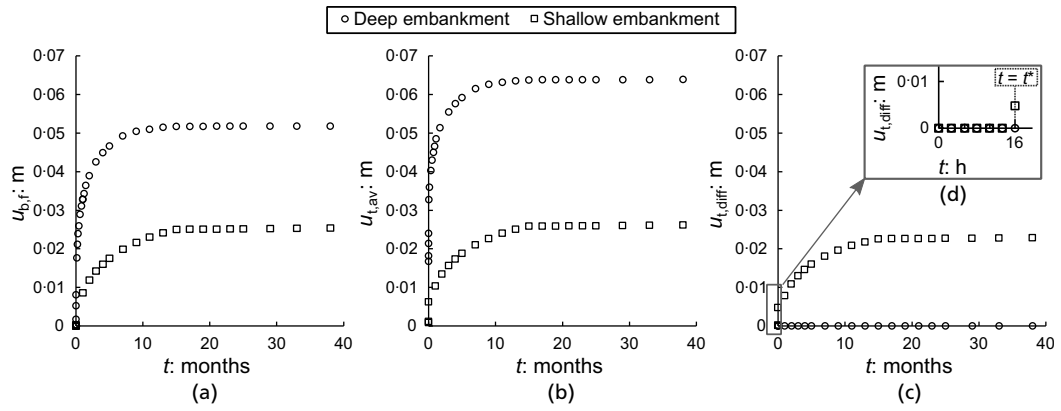


Fig. 2. Evolution during consolidation of: average settlements at (a) base and (b) top of the embankment; and (c) differential settlements at the top of the embankment. (d) Zooming in on the beginning of consolidation for the case of shallow embankment (SE)

settlements are nil for both SE and DE (Fig. 2(d)), meaning that the PES is in $z = 0$. During consolidation, for the DE case, $u_{t,diff} = 0$ and $u_{b,f} > 0$, meaning that the distance of the PES from the embankment base (h^*) evolves with time within the embankment body.

Process height

The process height (h_p in Fig. 3) is the height of the zone in the proximity of the pile edge where strains localise (di Prisco *et al.*, 2020). The evolution of the process zone during consolidation is reported as an original result in Figs 3

and 4. For both DE and SE, at $t = 0$, plastic shear strains are nil within the embankment (Figs 3(a) and 3(f)). During consolidation, plastic shear strains develop within the embankment in a narrow crown close to the edge of the pile head (Figs 3(c)–3(e) and 3(h)–3(j) for DE and SE, respectively). The h_p -long zone where the soil yields is the ‘process zone’ and reaches the top of the embankment only for SEs (Figs 3(h)–3(j)).

It is worth noticing that h_p is initially nil and remains nil for a not negligible time interval (Figs 3(a) and 3(b), and Figs 4(f) and 4(g)). During this period, the embankment soil does not exhibit any plastic strain and behaves

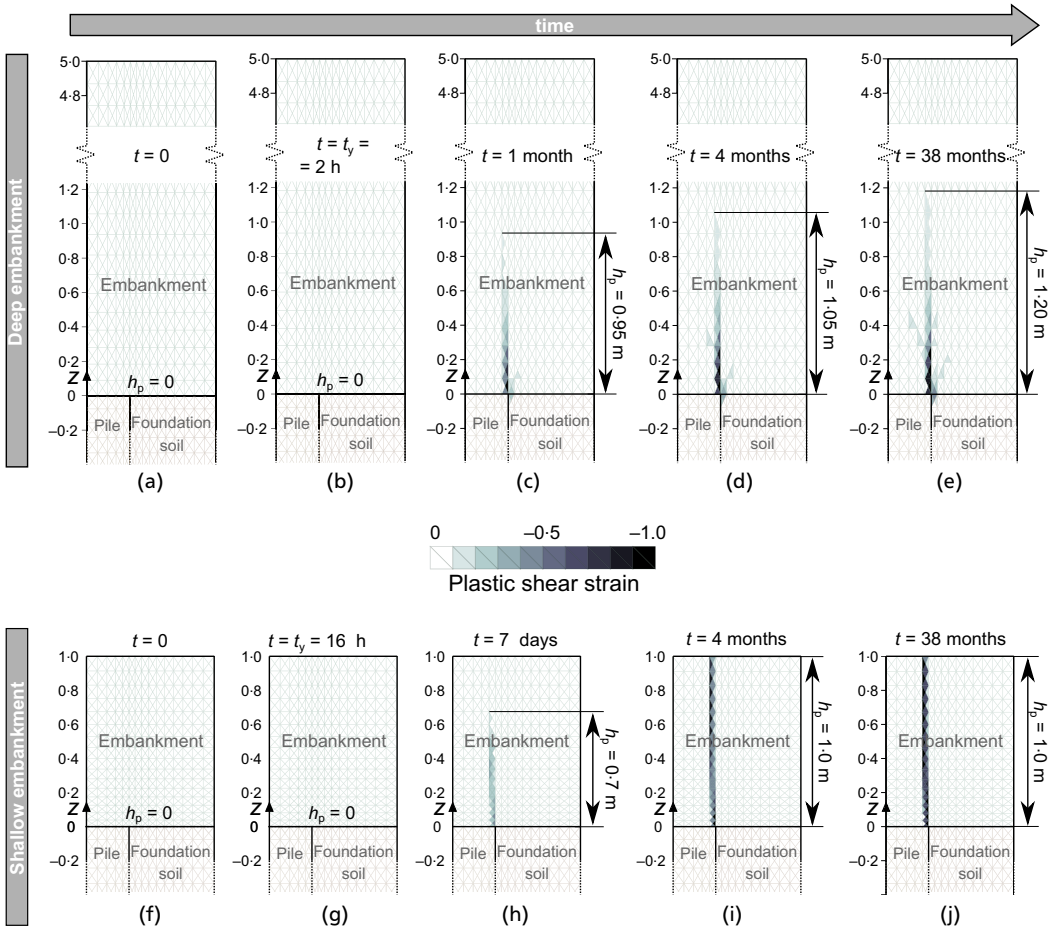


Fig. 3. Contour of plastic shear strains and of plastic (process) height, h_p , during consolidation for both the reference cases of (a)–(e) deep embankment (DE) and (f)–(j) shallow embankment (SE)

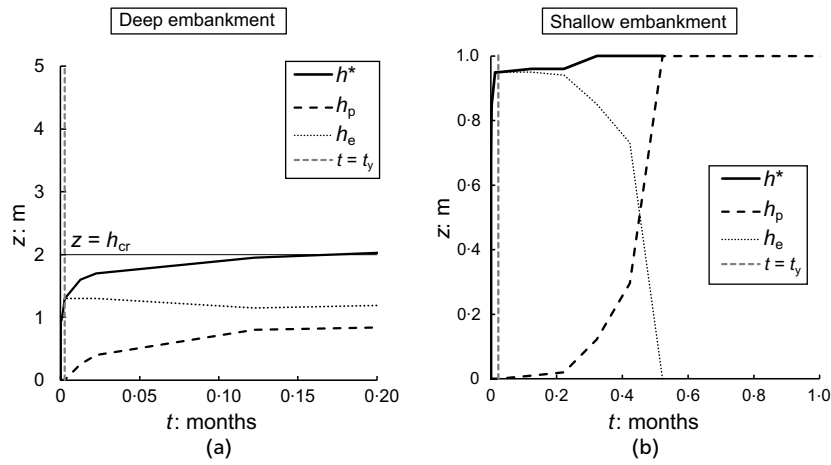


Fig. 4. Evolution with time of the height of the plane of equal settlements (PES), the process height and the elastic height for both (a) deep and (b) shallow embankments (SEs) at the beginning of consolidation

elastically. At $t = t_y$, yielding starts to take place and plastic strains, together with h_p , progressively start evolving until the end of consolidation.

For the sake of clarity, the evolution with time of both h^* (subsection 'Plane of equal settlements') and h_p , for both DE and SE, is illustrated in Fig. 4. The volume in between PES and the top of the process zone is an elastic zone of thickness $h_e = h^* - h_p$. For the DE case, h_e is almost constant after yielding (dotted line in Fig. 4(a)). For the SE case (Fig. 4(b)), h_p starts evolving after yielding, rapidly reaching the top of the embankment, and when $h_p = h$, the PES does not belong to the embankment any longer and $h_e = 0$.

The asymptotic value of h^* is the critical height (h_{cr}) in Fig. 4(a)). For DEs, $h > h_{cr}$, whereas, for SEs, for a sufficiently large time, $u_{t,diff} > 0$, the PES at the end of consolidation is not defined within the embankment domain and $h = h_p$.

Therefore, h_{cr} coincides with the minimum value of h for which, $u_{t,diff} = 0$ at the end of the consolidation process. This implies that h_{cr} is a function of the construction rate: for instance, considering the same reference DE, $h_{cr} = 1.5$ m if the embankment is constructed under drained conditions (i.e. very small values of construction rates, as in di Prisco *et al.* (2020)), whereas $h_{cr} = 2$ m (Fig. 4) under undrained construction conditions (i.e. very large values of construction rates).

Arching effect

Analogously to settlements, average values of the total vertical stress in $z = 0$ can be used to plot the evolution with time of stresses at the top of both concrete pile and soft soil:

$$\sigma_c = \frac{2\pi \int_0^{d/2} \sigma_v(r) dr}{\pi d^2/4}, \quad \sigma_f = \frac{2\pi \int_{d/2}^{s/2} \sigma_v(r) dr}{\pi (s^2 - d^2)/4} \quad (5)$$

being σ_v the total vertical stress at $z = 0$ along r .

For $t = 0$, for both DE and SE, $\sigma_c/\gamma h = \sigma_f/\gamma h = 1$ (Fig. 5). For $t > 0$, consolidation takes place and, due to the arching effect, σ_c progressively increases, while σ_f decreases. Furthermore, tangential stresses (τ in Figs 6(a) and 6(b), relative to DE and SE, respectively) increase during consolidation within the embankment close to the pile edge ($r = d/2$). Since τ is practically negligible above the PES ($z > h^*$), τ -isochrones numerically computed for $r = d/2$ in Fig. 6 refer only to $0 < z < h^*$. For the sake of clarity, $z =$

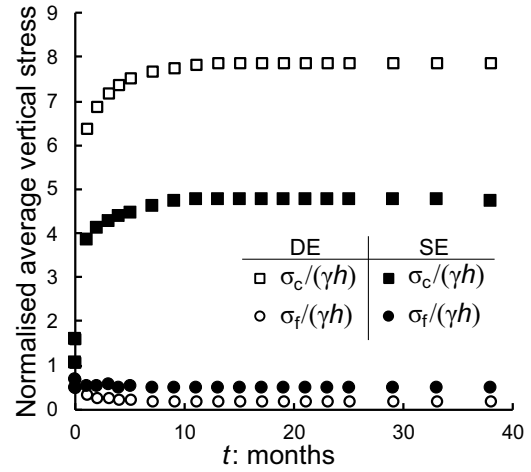


Fig. 5. Evolution during consolidation of normalised average total vertical stress acting over the concrete pile and the foundation soil for both deep embankment (DE) and shallow embankment (SE) reference cases

$h_p(t)$ (large black circles in Figs 6(a) and 6(b)) is reported on each of the isochrones to highlight that τ are transmitted within the elastic zone as well. The τ trend is dominated by the boundary condition in $z = 0$, where shear stresses have to be nil since the pile shaft is assumed to be smooth.

MATHEMATICAL MODELLING

In the light of the numerical results illustrated in the second section 'FE numerical results', in this section, a mathematical model is introduced, putting in relation embankment height and time with average and differential embankment settlements. With this aim, all the hypotheses listed in the previous section 'FE numerical results' for the definition of the numerical model are employed.

Sub-structuring approach

The mechanical response of the ideal axisymmetric unit cell (Fig. 1(b)) can be subdivided into an initial elastic phase ($0 < t < t^*$) and a subsequent elastic-plastic one ($t > t^*$). During the elastic phase, $h_p = 0$ (Figs 3(b) and 3(g)), the PES evolves upwards (h^* in Figs 4(a) and 4(b)). During the elastic-plastic phase, $h_p > 0$ (Figs 3(c)–3(e) and 3(h)–3(j))

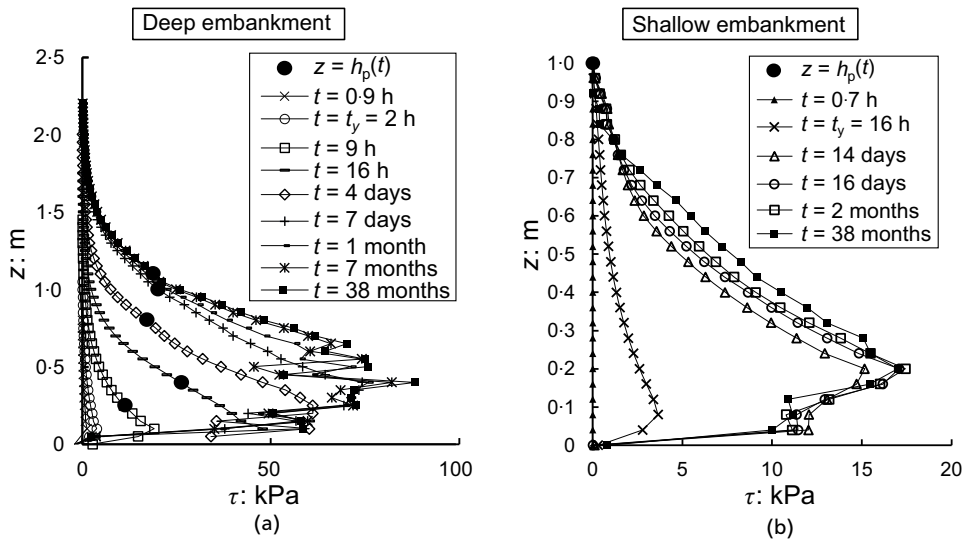


Fig. 6. Vertical profiles within the embankment of tangential stresses, τ , during consolidation for (a) deep embankment (DE) and (b) shallow embankment (SE) reference cases

and the evolution with time of h_e is different for DEs and SEs. In the former case, h_e initially increases until it reaches an almost constant value ($t > t^*$ in Fig. 4(a)), whereas, in the latter one, h_e initially increases until a plateau (at which $h_e = h^*$), but, subsequently, it progressively nullifies (Fig. 4(b)).

The model hereafter assumes sub-structuring the spatial domain into eight zones, whose thickness evolves over time, due to the almost constant trend along r of both settlements and vertical stresses for $0 < r < d/2$ and $d/2 < r < s/2$. In Fig. 7, where $Z = z/d$ is the non-dimensional vertical coordinate, element number:

- (a) 1 corresponds to the concrete pile, modelled as a rigid element
- (b) 2 corresponds to the foundation soil, modelled as a viscous-elastic element

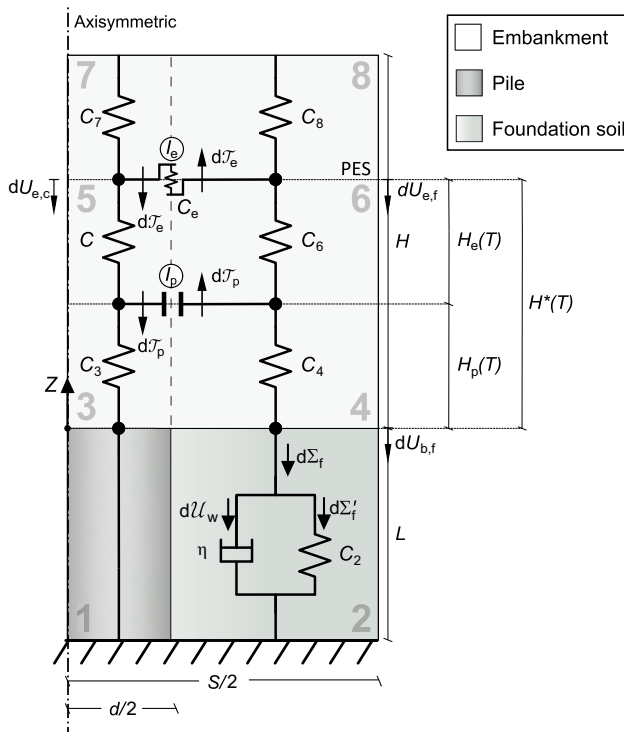


Fig. 7. Complete mathematical model scheme

- (c) 3 and 4 correspond to embankment subdomains modelled as elastic elements, whose height evolves with h_p (geometrical non-linearity)
- (d) 5 and 6 correspond to embankment subdomains modelled as elastic elements, whose height evolves with h_e (geometrical non-linearity)
- (e) 7 and 8 correspond to embankment subdomain modelled as elastic elements, whose height reduces with both h_e and h_p increasing (geometrical non-linearity).

Subdomains 7 and 8 do not interact to each other, since there is no transfer of shear stresses along their interface (Fig. 6). The shear stress transfer at the interface between subdomains 5 and 6 has been modelled by means of an elastic interaction element located at $z = h^*(t)$ (I_e in Fig. 7), whereas a plastic interaction element (I_p in Fig. 7) is used at $z = h_p(t)$ to model the stress transfer through the process zone (between subdomains 3 and 4). Subdomains 1 and 2 do not interact with each other since the pile is assumed to be smooth.

Each element in Fig. 7 is assumed to deform only vertically, due to axisymmetric conditions. Horizontal stresses in elements 4 and 6 are used to calculate shear stresses along vertical interfaces (as detailed in the subsection 'Vertical stress redistribution system').

Mathematical model

The mathematical model is conceived by using non-dimensional variables (di Prisco *et al.*, 2020):

$$U_{b,f} = \frac{u_{b,f}}{l} \frac{E_{oed,f}}{\gamma d}, \quad U_{t,diff} = \frac{u_{t,diff}}{l} \frac{E_{oed,f}}{\gamma d}, \quad U_{t,av} = \frac{u_{t,av}}{l} \frac{E_{oed,f}}{\gamma d} \quad (6)$$

where $E_{oed,f}$ is the foundation soil elastic oedometric stiffness, and the average stresses:

$$\Sigma_f = \frac{\sigma_f}{\gamma d}, \quad \Sigma_c = \frac{\sigma_c}{\gamma d} \quad (7)$$

In agreement with one-dimensional (1D) consolidation theory, the non-dimensional time:

$$T = \frac{k_v E_{oed,f}}{\gamma_w l^2} t \quad (8)$$

where k_v is the foundation soil vertical hydraulic conductivity and γ_w is the water unit weight, is used.

Using non-dimensional variables is particularly convenient since, in the non-dimensional $U_{t,\text{diff}} - T$ and $U_{t,\text{av}} - T$ planes, the embankment response is unique if: (a) the non-dimensional geometrical ratios ($H = h/d$, $S = s/d$, $L = l/d$); (b) the non-dimensional stiffness ratio ($E_{\text{oed,f}}/E_{\text{oed,e}}$, where $E_{\text{oed,e}}$ is the oedometric modulus of the embankment); (c) friction and dilatancy angle values, ϕ'_e and ψ_e ; and (d) $(k_v E_{\text{oed,f}})/(\gamma_w l^2)$ are kept constant.

The constitutive relationships expressed in terms of the previously listed non-dimensional variables are a function of the non-dimensional compliances (Fig. 7) listed here below:

$$C_2 = \frac{L}{E_{\text{oed,f}}} \frac{E_{\text{oed,f}}}{L} = 1 \quad (9)$$

$$C_3 = C_4 = \frac{H_p(T)}{E_{\text{oed,e}}} \frac{E_{\text{oed,f}}}{L} \quad (10)$$

$$C_5 = C_6 = \frac{H_e(T)}{E_{\text{oed,e}}} \frac{E_{\text{oed,f}}}{L} \quad (11)$$

$$C_7 = C_8 = \frac{H(T) - H_p(T) - H_e(T)}{E_{\text{oed,e}}} \frac{E_{\text{oed,f}}}{L} \quad (12)$$

being $H_p = h_p/d$ and $H_e = h_e/d$ the non-dimensional h_p and h_e , respectively. The evolution of the non-dimensional height of PES ($H^*(T) = H_p(T) + H_e(T)$) is discussed in the subsection later in this paper 'Evolution of hidden variables'.

The non-dimensional shear forces, \mathcal{T}_e and \mathcal{T}_p , (transferred by I_e and I_p , respectively) are:

$$\mathcal{T}_e = \frac{\pi \int_{h_p}^{h_p+h_e} \tau(z) dz}{\gamma d^2} \quad (13)$$

$$\mathcal{T}_p = \frac{\pi \int_0^{h_p} \tau(z) dz}{\gamma d^2} \quad (14)$$

By considering (a) balance of momentum along vertical direction; (b) constitutive laws of all elements of Fig. 7 and interfaces (I_e and I_p); and (c) compatibility conditions along z , the generalised constitutive relationship (taking into consideration not only the consolidation process taking place for $t > 0$, but also the embankment construction time period) for the geo-structure can be written as:

$$\begin{Bmatrix} dU_{t,\text{av}} \\ dU_{t,\text{diff}} \end{Bmatrix} = \begin{Bmatrix} C_{\text{av}}(\chi, H) & \Phi_{\text{av}}(\chi, H) \\ C_{\text{diff}}(\chi, H) & \Phi_{\text{diff}}(\chi, H) \end{Bmatrix} \begin{Bmatrix} dH \\ dT \end{Bmatrix} \quad (15)$$

where C_{av} and C_{diff} are non-dimensional compliances; Φ_{av} and Φ_{diff} are non-dimensional average and differential settlement rates related to the consolidation of the foundation soil (see subsection 'Vertical stress on foundation soil and concrete pile'). The expressions for both compliances and settlements rates (reported in the Appendix), are obtained by employing the scheme of Fig. 7 and the constitutive relationships given in both of the next two subsections 'Vertical stress redistribution mechanism' and 'Vertical stress on foundation soil and concrete pile'.

In equation (15), $dU_{t,\text{av}}$ and $dU_{t,\text{diff}}$ are the output variables and dH is the loading variable, whereas χ is the vector containing the 'hidden variables' (whose evolution is defined in the subsection 'Vertical stress on foundation soil and concrete pile'):

$$\chi = \{\mathcal{U}_w, H_e, H_p\}^T \quad (16)$$

where \mathcal{U}_w represents the non-dimensional average stresses acting on the dashpot of subdomain 2, related to the excess pore pressure in the foundation soil.

Vertical stress redistribution mechanism

Shear stresses transmitted by I_e and I_p increase with time due to the increase in $U_{b,f}$ during consolidation. As suggested by Fig. 3, the shear stress transfer process is initially elastic and, in a second phase, elastic-plastic.

In the mathematical model, during the elastic phase, the non-dimensional shear forces are transmitted only by I_e (see the following subsection 'Elastic phase'), whereas they are transmitted by both I_e and I_p during the elastic-plastic one (see subsection 'Elastic-plastic phase').

Elastic phase. During the elastic phase, subdomains 3 and 4 are not defined ($H_p = 0$, from Figs 3 and 4). When consolidation starts, $U_{b,f}$ increases, whereas the top of the pile does not move. Therefore, $U_{b,f}$ coincides with non-dimensional differential displacements at the embankment base, and:

$$\mathcal{T}_e = \frac{U_{b,f}}{C_e} \quad (17)$$

where C_e is a generalised elastic embankment compliance, calibrated on FE method numerical results in the later subsection 'Mathematical model calibration'.

Equation (17) holds until the maximum shear stress within the elastic zone, τ_0 (Fig. 8, where $Z = z/d$ is the non-dimensional vertical coordinate) reaches the value of yielding, τ_{pl} :

$$\frac{\tau_{\text{pl}}}{\gamma d} = \frac{\gamma h \bar{k} \tan \phi'_{ss}}{\gamma d} = H \bar{k} \tan \phi'_{ss} \quad (18)$$

where both vertical and horizontal stresses are assumed to increase linearly with depth and are related to each other by a constant ratio \bar{k} , whose dependence on ψ_e is calibrated on FE method numerical results in the subsection 'Mathematical model calibration', whereas:

$$\tan \phi'_{ss} = \frac{\cos \psi_e \sin \phi'_e}{1 - \sin \psi_e \sin \phi'_e} \quad (19)$$

where ϕ'_{ss} is the embankment soil friction angle under simple shear conditions (di Prisco *et al.*, 2020).

By assuming a parabolic distribution of tangential stresses at the interface (as suggested by Fig. 6, for $t < t^*$), the maximum value of $\tau/\gamma d$ along depth (Fig. 8(a)) is:

$$\frac{\tau_0}{\gamma d} = \frac{3}{\pi H_e} \mathcal{T}_e \quad (20)$$

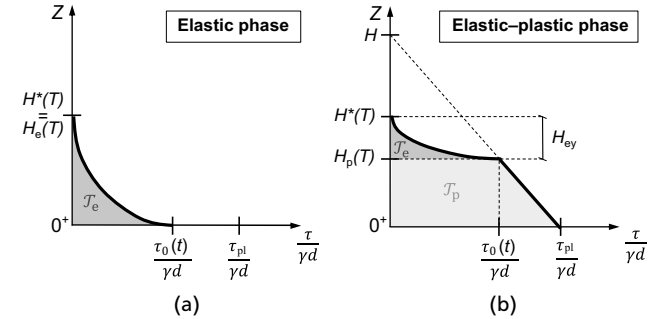


Fig. 8. Non-dimensional tangential stresses transmitted at the interface along Z during consolidation for both the (a) elastic and (b) elastic-plastic phases

By substituting equation (18) into equation (20):

$$\tau_{ey} = \frac{\pi H \bar{k} \tan \phi'_{ss}}{3} H_e \quad (21)$$

the value of τ_e at yielding ($\tau_0 = \tau_{pl}$) is obtained.

Elastic–plastic phase. In the elastic–plastic phase, $d\tau_e$ is calculated by assuming, for the distribution of $\tau/\gamma d$ along depth: (a) $dH_e = 0$ (see subsection ‘Sub-structuring approach’) and (b) a parabolic shape for $Z > H_p$ (Fig. 8(b)):

$$d\tau_e = \pi \bar{k} \tan \phi'_{ss} \frac{H_{ey}}{3} \left(dH - \frac{dH_p}{2} \right) \quad (22)$$

where H_{ey} is the (constant) value of H_e at yielding ($t = t^*$).

Since, for $0 < Z < H_p$, both vertical and horizontal stresses at yielding are assumed to depend linearly on depth (Fig. 8(b)), and shear stress to be calculated according to the Mohr–Coulomb failure criterion:

$$d\tau_p = \pi \bar{k} \tan \phi'_{ss} \left[H_p dH + \left(H - \frac{H_p}{2} \right) dH_p \right] \quad (23)$$

Vertical stress on foundation soil and concrete pile

Owing to the FE model simplifications, consolidation in the soft soil evolves one-dimensionally. Therefore, a simplified Kelvin–Voight model is used in subdomain 2 and:

$$\Sigma_f = \Sigma'_f + U_w \quad (24)$$

where

$$\Sigma'_f = U_{b,f}/C_2 \quad (25)$$

$$U_w = \eta \frac{dU_{b,f}}{dT} \quad (26)$$

The non-dimensional pseudo-viscous parameter, η , mimics the temporal evolution of excess pore water pressure during consolidation in a saturated homogeneous soil stratum. In the non-dimensional space, $\eta = 1/3$ fits the evolution with time of settlements at the top of the foundation soil that would be obtained for 1D consolidation under a constant total vertical

stress according to Terzaghi’s theory and is independent from the soil mechanical properties, hydraulic conductivity and geometry of the system.

By computing the balance of momentum along the vertical direction of the embankment according to the scheme of Fig. 7, the evolution of average vertical stresses is obtained:

$$\begin{aligned} d\Sigma_f &= dH - \frac{4}{\pi(S^2 - 1)} (d\tau_e + d\tau_p); \\ d\Sigma_c &= dH + \frac{4}{\pi} (d\tau_e + d\tau_p) \end{aligned} \quad (27)$$

where $d\tau_e$ and $d\tau_p$ are evaluated differently during the elastic phase (equation (17), whereas $d\tau_p = 0$) and the elastic–plastic phase (equations (22) and (23)).

Evolution of hidden variables

The evolution of hidden variables χ (equation (16)) can be written as follows:

$$d\chi = \mathbf{F} \begin{Bmatrix} dH \\ dT \end{Bmatrix} = \begin{Bmatrix} F_{11} & F_{12} \\ F_{21} & F_{22} \\ F_{31} & F_{32} \end{Bmatrix} \begin{Bmatrix} dH \\ dT \end{Bmatrix} \quad (28)$$

where:

$$\mathbf{F} = \begin{cases} \mathbf{F}^e \text{ if } \tau_e < \tau_{ey} \\ \mathbf{F}^{ep} \text{ if } \tau_e = \tau_{ey} \end{cases} \quad (29)$$

in which:

$$\mathbf{F}^e = \begin{cases} 1 & -\frac{4 + \pi C_e (S^2 - 1) U_w}{\pi C_e (S^2 - 1)} \frac{\eta}{\eta} \\ 0 & \frac{H_e F_{12}^e}{(H - U_w)} + \frac{E_{oed,e} L [\pi C_e (S^2 - 1) + 4]}{4 S^2 E_{oed,f} (H - U_w)} \frac{U_w}{\eta} \\ 0 & 0 \end{cases} \quad (30)$$

and

$$\mathbf{F}^{ep} = \begin{cases} 1 - \frac{2 \bar{k} \tan \phi'_{ss} [(H_{ey} + 3H_p)(2 - F_{31}^{ep}) + 6HF_{31}^{ep}]}{3(S^2 - 1)} & -\frac{U_w}{\eta} - \frac{2 \bar{k} \tan \phi'_{ss} (6H - 3H_p - H_{ey}) F_{32}^{ep}}{3(S^2 - 1)} \\ 0 & 0 \\ F_{31}^{ep} & F_{32}^{ep} (H - H_p)^0 \end{cases} \quad (31)$$

where

$$F_{31}^{ep} = \frac{4 (H_{ey}^2 + 3H_p^2 + H_{ey}H_p)}{3H_p(3H_p - 8H) + 2H_{ey}(2H_p - 2H + H_{ey})} \quad (32)$$

$$F_{32}^{ep} = -\frac{\mathcal{U}}{\eta} \frac{3L E_{oed,e} (S^2 - 1)}{S^2 E_{oed,f} \bar{k} \tan \phi'_{ss} \{3(3H_p - 8H)H_p + 2(H_{ey} + 2H_p - 2H)H_{ey}\}}. \quad (33)$$

The Macaulay's bracket multiplying F_{32}^{ep} in equation (31) includes the case of SE, where H_p stops evolving ($F_{32}^{\text{ep}}(0)^0 = 0$) when reaching the top of the embankment ($H_p = H$).

The increment of the hidden variable U_w is evaluated by (a) substituting equation (24) into equation (25); (b) computing the time derivative of the obtained equation and (c) substituting equations (26) and (27) in this one. The increment of both H_e and H_p is evaluated by using both the following conditions:

$$dU_{e,\text{diff}} = 0 \quad (34)$$

$$dH_e dH_p = 0 \quad (35)$$

where $dU_{e,\text{diff}}$ is obtained from the balance of momentum, the compatibility and the constitutive equations in accordance with the scheme in Fig. 7, the increment of differential settlements at the PES.

Mathematical model calibration

The mathematical model requires the assessment of $C_e(E_e/E_f)$ and $\bar{k}(\psi_e)$. The generalised non-dimensional embankment compliance, C_e (equation (17)), is evaluated from FE numerical results by estimating both $U_{b,f}$ and T_e at the beginning of the elastic phase. Thanks to its non-dimensional definition, C_e is numerically observed to depend only on the relative embankment–foundation soil stiffness (E_e/E_f , where E_e and E_f are the Young's moduli of the embankment and foundation soil, respectively). This dependence is illustrated in Fig. 9(a). Since $E_e/E_f < 10$, cases are not common for engineering applications, C_e is assumed to be constant and equal to 1.76×10^{-3} . This implies that the model may not be suitable for predicting the system response

of piled embankments on foundation soils that are not sufficiently soft.

For the sake of simplicity, in equations (18) and (21)–(23), \bar{k} is considered to be constant during the consolidation process and only to depend on ψ_e . The function $\bar{k}(\psi_e)$ is obtained from FE numerical results by calculating the average value of $k = \sigma_h/\sigma_v$ for $0 < z < h_p$ at the end of the consolidation process. In Fig. 9(b), both FE numerical results and the expression employed in the mathematical model to interpolate them are reported.

MODEL PERFORMANCE

The numerical integration of the mathematical model requires the definition of the construction sequence, geometry and the standard hydro-mechanical properties of soil (all the necessary input data are listed in the first line of Table 3). Equations (15)–(39) have been integrated/implemented by using Matlab (2022) software.

For the sake of generality, the mathematical model is conceived to simulate any embankment construction rate, that is also 'partially drained' embankment construction. Nevertheless, for the sake of brevity, in this section and in the following one, the embankment construction is always assumed to take place under undrained conditions. In the section 'Validation on experimental data and other numerical studies', the effects of construction velocity are discussed.

Comparison with numerical results

In this paragraph, the predictions of the mathematical model are compared with FE results for the DE reference case (Fig. 1(b), Tables 1 and 2). In particular, in Figs 10(a)

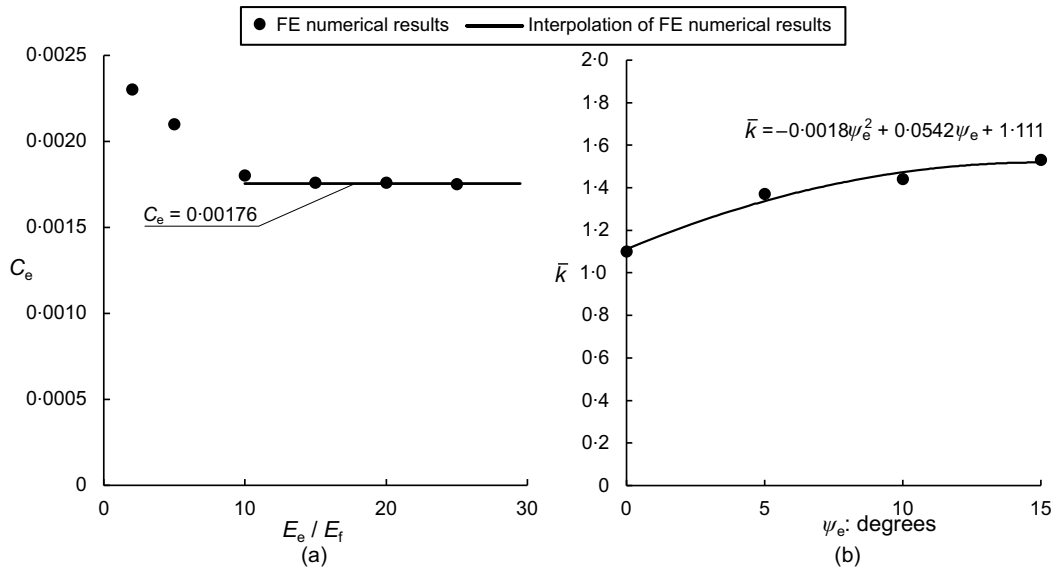


Fig. 9. Calibration of (a) C_e and (b) \bar{k} against finite element (FE) numerical results obtained by considering the model introduced in Fig. 1(b)

Table 3. Geometry and material properties used in the mathematical model for the validation against the full-scale experiment of Briançon & Simon (2012). S is calculated as in McGuire (2011) for piles with a squared pattern

Test from reference	d : m	s : m	l : m	h : m	$E_{f,\text{soed}}$: MPa	E_e : MPa	ϕ'_e : deg	ψ_e : deg	γ : kN/m ³	k_v : m/s
Briançon & Simon (2012)	0.38	2.83	7.5	5	4	10	20	36	18.5	3.2×10^{-8}
Liu <i>et al.</i> (2023)	0.5	3.54	15	8	0.8		30	34	23	1.5×10^{-7}

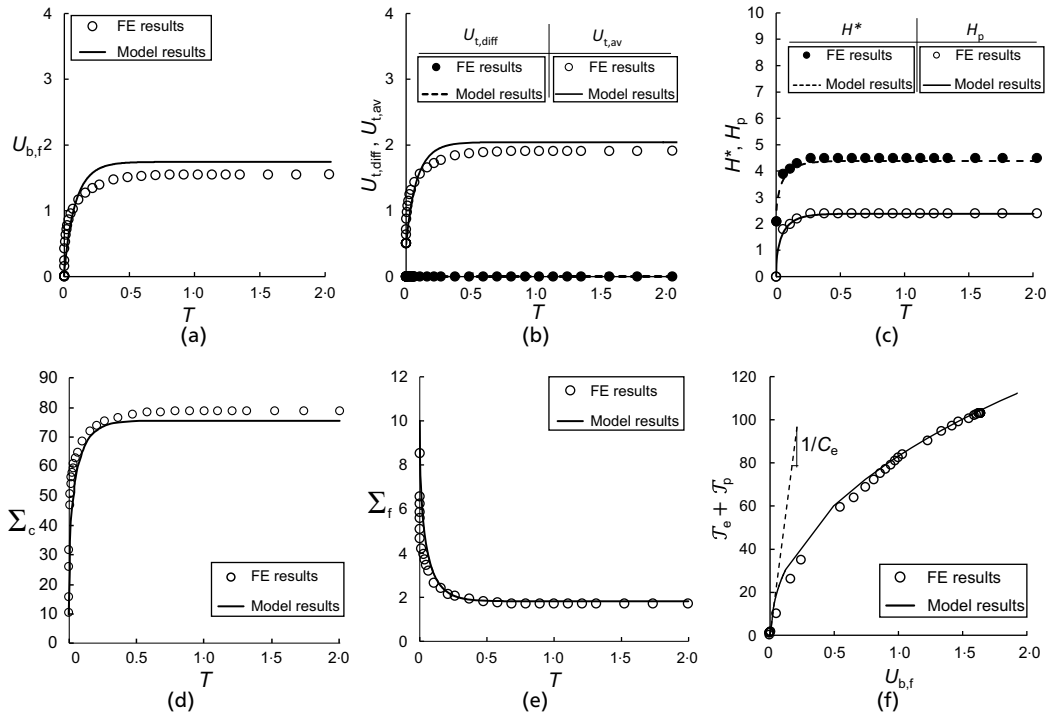


Fig. 10. Comparison, for deep embankment (DE) reference case, between numerical results and mathematical model predictions during consolidation in terms of non-dimensional settlements at the (a) base and (b) top of the embankment; (c) plane of equal settlements (PES) height and process height; average vertical stress acting on the (d) concrete pile and (e) foundation soil; (f) transferring force plotted against non-dimensional settlements at the base of the embankment

and 10(b) the comparison concerns non-dimensional settlements. The agreement is very satisfactory both qualitatively and quantitatively. In Figs 10(c) and 10(f), the evolution with time of all the variables that can be extracted from the model are compared against FE results (H^* , H_p , Σ_c , Σ_f with time and $(T_e + T_p)$ with $U_{b,f}$). As is evident in Figs 10(d) and 10(e), the mathematical model satisfactorily reproduces the evolution of vertical average stress in $z = 0$ due to the arching effect occurring during consolidation. Analogously (Fig. 10(d)), also well captured is the reduction in the non-dimensional stiffness of $(T_e + T_p) - U_{b,f}$ curve from the initial value (corresponding to $1/C_e$), due to both yielding in the process zone and its upwards propagation.

To further assess the mathematical model's capability of reproducing FE numerical results, the authors performed a parametric study (by changing both geometry and mechanical properties) and summarised the results obtained in terms of average settlements ($u_{t,av}$ and $u_{b,f}$) and stresses (σ_f and σ_c) at the end of consolidation in Fig. 11. The agreement between mathematical model predictions and FE results is satisfactory: the R -squared value for $u_{t,av}$, $u_{b,f}$ and σ_f is 0.99, whereas it is 0.98 for σ_c .

Particularly good is the agreement in terms of $u_{t,av}$ and σ_c . The quality of predictions reduces for increasing values of s/d . For $s/d > 6$ (corresponding to an area replacement ratio lower than 2.7%), the overestimation of $u_{t,av}$, $u_{b,f}$, σ_f and σ_c is larger than 10%. This is justified by the evolution of the geometry of the process zone observed from numerical results. In fact, as already commented by King *et al.* (2019), for sufficiently large s/d values, the process zone stops being vertical and unique, as assumed in the mathematical model proposed in this paper. However, even in these cases, the mathematical model provides a conservative estimation of settlements at the top.

Particularly satisfactory is the comparison for the SE reference case (empty circles in Fig. 11).

Validation on experimental data and other numerical studies

The hypotheses introduced to generate the FE numerical results, from which the mathematical model is derived, are particularly restrictive (axisymmetric conditions, smooth shaft piles and embankment construction under undrained conditions). Hence, experimental test results that perfectly fit the problem numerically solved are not available in literature. Thus, after its validation on the results of a numerical parametric study presented herein, the authors further benchmarked the model against data from experiments and other numerical analyses from the literature (that fit most of the hypotheses formulated in this study) to validate the mathematical model, without pretending to perfectly reproduce the measurements. Many researchers have investigated soil arching in several field case studies (e.g. Oh & Shin, 2007; Van Duijnen *et al.*, 2010; Van Eekelen *et al.*, 2010; Briançon & Simon, 2012; Lu *et al.*, 2013, 2020; Xing *et al.*, 2014; van Eekelen *et al.*, 2020; Feng *et al.*, 2021) or lab tests (Jenck *et al.*, 2007; van Eekelen *et al.*, 2012; Okyay *et al.*, 2014; Girout *et al.*, 2016; Yu *et al.*, 2021; Liu *et al.*, 2023). However, in almost all these cases, geosynthetic reinforcement layers (not considered in this study) were placed at the embankment base or the effects of the consolidation process (which are the focus of this study) were not appreciable. Furthermore, lab tests are usually performed either to explore the behaviour at failure of piled embankments or to validate ultimate limit state analytical methods. Consequently, the stiffness properties of the soil in the embankment and foundation (essentials for this study) are not provided.

The mathematical model proposed is validated against both a full-scale experiment from Briançon & Simon (2012) and a centrifuge test from (Liu *et al.*, 2023), as both consider

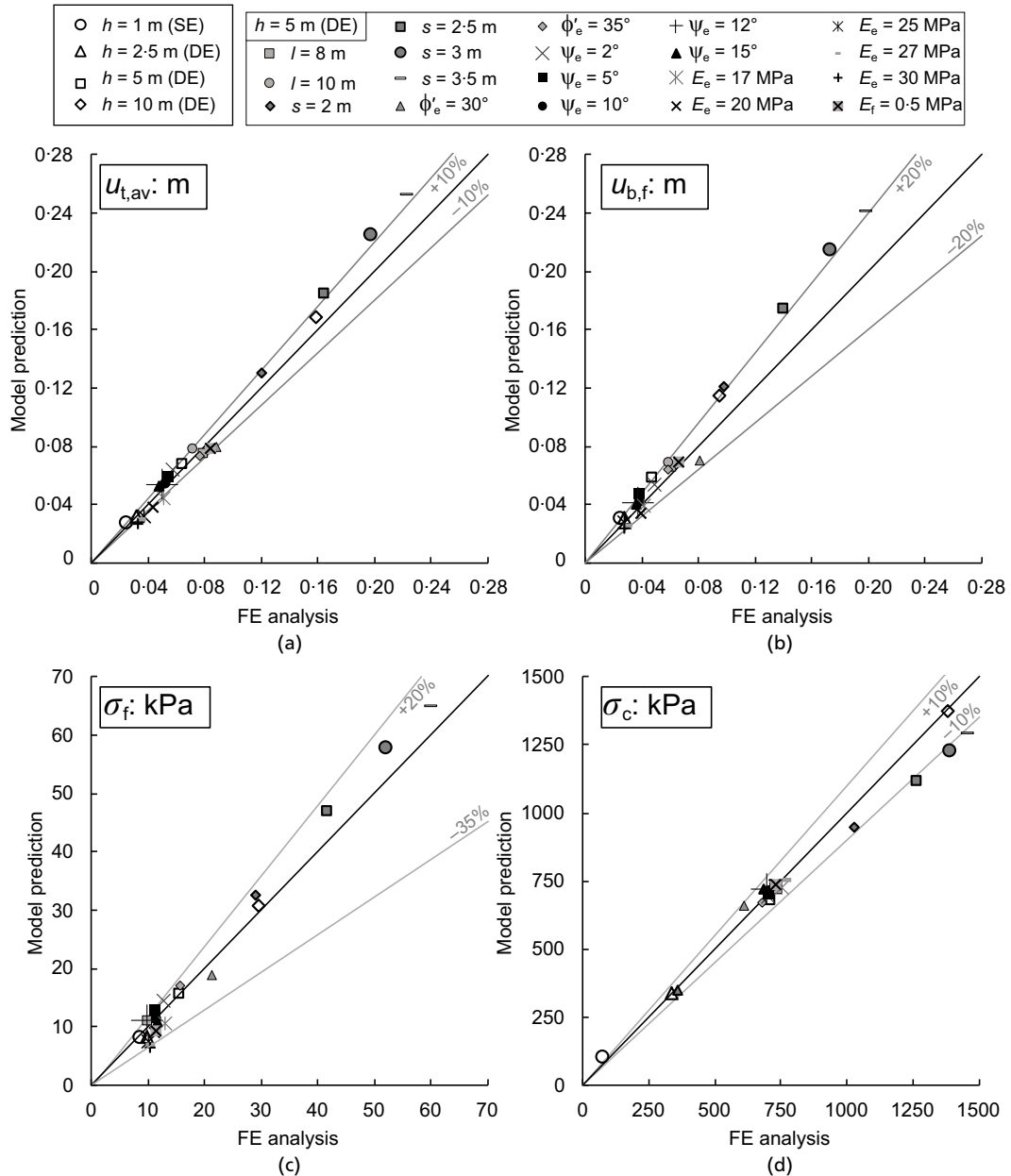


Fig. 11. Comparison of mathematical model predictions and numerical simulations at long-term conditions in terms of: average settlements at the (a) top and (b) base of the embankment; average vertical stresses on the (c) foundation soil and (d) concrete pile (geometry and mechanical properties not indicated in the legend are reported in Tables 1 and 2)

end-bearing piles surrounded by a saturated clayey material. In addition, both tests report the results of a reference case without piles and geosynthetics, which was fundamental for estimating the stiffness value of the foundation soil from the stress and settlement at the base of the embankment at the end of consolidation (secant modulus at the end of consolidation of the foundation soil).

The study from Briançon & Simon (2012) was numerically modelled by Rowe & Liu (2015) and Nunez *et al.* (2013), who both performed 3D numerical analyses to reproduce the mechanical behaviour of the test. The numerical scatter characterising 3D numerical results is emphasised in Fig. 12(a), where the final value at the base predicted by Nunez *et al.* (2013) (black dot) is compared to the numerical results by Rowe & Liu (2015) (dark grey line) in terms of settlements at the midspan between piles at the embankment base.

For the validation of the mathematical model, the input data from Rowe & Liu (2015) are used (see Table 3 and

black continuous line in Fig. 12(a)), except for the l value, which is taken from Briançon & Simon (2012). Given the sophisticated constitutive models employed in the numerical study from Rowe & Liu (2015), the oedometric secant modulus of the soft soil layer was estimated as secant modulus from the interpretation of the numerical results relative to the section without piles. The nil embankment fill dilatancy assumed in Rowe & Liu (2015) corresponds to $\bar{k} = 1.1$ (Fig. 9).

The results of the mathematical model (solid lines in Figs 12(a) and 12(b)) are compared against measurements from Briançon & Simon (2012) (grey crosses in Figs 12(a) and 12(b)) and (when available) numerical results from Nunez *et al.* (2013) and Rowe & Liu (2015) in terms of (a) settlements (Fig. 12(a)) and stresses (Fig. 12(b)) at the base of the embankment, at the midspan between piles, (b) stresses on the pile, measured at 0.5 m depth (Fig. 12(b)), and (c) differential and average settlements at the top of the embankment (Table 4), accumulated in Rowe & Liu (2015)

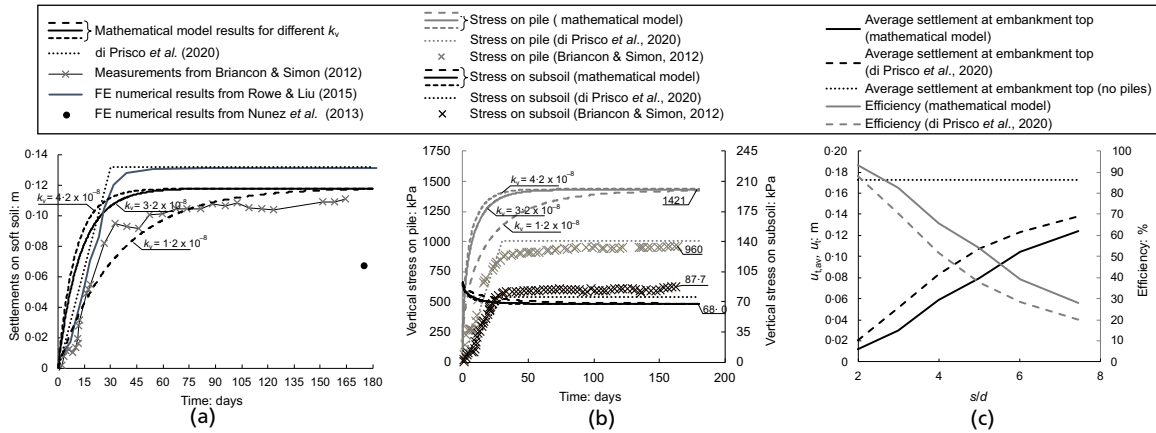


Fig. 12. Validation of the mathematical model in terms of: (a) evolution of settlements at the top of the foundation soil; (b) evolution of stresses over the pile and foundation soil against both measurements of the full-scale experiment by Briançon & Simon (2012) and numerical results by Rowe & Liu (2015) and Nunez *et al.* (2013); (c) $u_{t,av}$ and efficiency of building piles in terms of average settlement at the top of the embankment under both drained and undrained embankment construction conditions, for different values of s/d for the case of Briançon & Simon (2012) (Table 3)

Table 4. Validation of the mathematical model in terms of settlements both at the top of the embankment, as calculated numerically by Rowe & Liu (2015) for $l = 9.5$ m, and at the base of the embankment, as measured by Liu *et al.* (2023), at the end of consolidation

	Rowe & Liu (2015)	Liu <i>et al.</i> (2023)	
	$u_{t,av}$: m	$u_{t,diff}$: m	Settlement of the soft soil: m
Literature value	0.029	0	
Model prediction	0.047	0	1.66
Error	61%	0%	-2.2%
			1.70
			1.18
			-31%

from the construction of the last layer of the embankment (corresponding to day 28) and the end of consolidation. $u_{b,f}$ (Fig. 12(a)) is calculated with equation (6) and integrating equations (26) and (28), whereas for $u_{t,av}$ and $u_{t,diff}$ in Table 4, equations (15) and (6) are used. σ_f and σ_c (Fig. 12(b)) are estimated by using equation (7) and integrating equations (27). Under the assumption of instantaneous embankment construction, the stresses calculated by the model start from a value corresponding to the weight of the embankment, uniformly distributed over the entire surface (pile + subsoil). To show how the model is affected by hydraulic conductivity, several values of k_v were considered (dashed lines in Figs 12(a) and 12(b)) and, for the sake of clarity, model results obtained by assuming the embankment construction under drained conditions (corresponding to $k_v \rightarrow \infty$) (di Prisco *et al.*, 2020) are added (dashed lines in Figs 12(a) and 12(b)).

Comparing the current model predictions with experimental data (grey crosses) and previous numerical results obtained by Rowe & Liu (2015) and Nunez *et al.* (2013), it is evident that despite the simplified assumptions employed in the model definition (which were not fully satisfied by the experimental setting) the present mathematical model simulation performs reasonably well. Regarding the final settlement (Fig. 12(a)), the current model shows an error of +7% compared with measurements, which is a good result if compared with the +19% error of Rowe & Liu (2015) and the -39% error of Nunez *et al.* (2013).

The observed discrepancies in Fig. 12(b) and Table 4 can be attributed to: (a) the sloping base of the soft layer observed in situ; (b) the assumption of smooth piles made in the mathematical model; (c) the differences in the constitutive laws; (d) geometric modelling (3D as opposed to axisymmetric conditions, as already commented upon by Bhasi & Rajagopal (2015)); and (e) construction rate implemented

in the numerical modelling of the test. The role of construction rate seems to be confirmed by the evolution with time of stresses on the subsoil: they continuously increase with time in the experiment, while model results are characterised by a continuous reduction due to consolidation. This is comparable with the results obtained by assuming the construction is taking place under drained conditions. It is also important to note that the comparison in terms of stresses over the pile involves average quantities from the model with local measurements from the experiment. Ideally, measurements of stress at the bottom of the pile would be more suitable for comparison with the model results. The mathematical model provides a reasonable (and quick) prediction of the settlements, also demonstrating that, despite its simplicity, the constitutive modelling adopted is representative of the mechanical behaviour of the system.

To put in evidence the role of drainage during embankment construction, Fig. 12(c) compares $u_{t,av}$ for different values of pile spacing, by using all input data in Table 3 and considering $k_v \rightarrow \infty$ (dashed black line) and $k_v = 3.2 \times 10^{-8}$ (solid black line), with the settlement at the top of the embankment without piles, u_t (dashed black line). The efficiency at the long term of building piles under different construction rates is calculated as $(u_{t,av} - u_t)/u_t$ for any s/d value (grey lines in Fig. 12(c)). For this specific case, the difference between the solid and the dashed grey lines ranges from 10 to 30%.

The model was further validated against the results of a centrifuge test from Liu *et al.* (2023). The input data for the mathematical model (Table 3) were taken from Liu *et al.* (2023), except for the stiffness modulus of the embankment that is difficult to evaluate in the lab and has been here assumed realistically ranging between 10 \div 30 MPa. For the two values of E_c , $u_{b,f}$ model predictions at the end of consolidation are compared in Table 4 with experimental data.

The minimum absolute error is 2.2% (for $E_e = 10$ MPa) and the maximum is 30.4% (for $E_e = 30$ MPa).

DISCUSSION AND COMPARISON WITH EXISTING FORMULAS

In the design of pile supported embankments a fundamental issue concerns the assessment of the critical height, since it defines whether differential settlements will be accumulated at the top of the embankment or not (SE or DE). The minimum embankment height needed to prevent differential settlements at the top of the embankment at the end of consolidation is the non-dimensional critical embankment height ($H_{cr} = h_{cr}/d$). Very popular to evaluate H_{cr} are the formulas suggested by BS 8006-1 (BSI, 2010) and McGuire (2011), where H_{cr} is a function only of pile spacing and diameter, but not of embankment and soft soil properties.

The formulas by BS 8006-1 (BSI, 2010), ASIRI (2012) and McGuire (2011) in the H_{cr} - S plane correspond to two different straight lines (dashed lines in Fig. 13(a)) separating the boundary between DEs and SEs. As is evident in Fig. 13(a), McGuire's formula is more conservative than the BS 8006-1's one.

In both the FE results and mathematical model predictions, the distinction between DEs and SEs is also a function of E_e/E_f (Fig. 13(a)). To highlight this, two different E_e/E_f values are considered as an example. As is evident, for small values of S , mathematical model predictions are very close to the BS 8006-1 formula, whereas for larger S values and sufficiently large E_e/E_f values, the mathematical model predictions approach McGuire's line.

The mathematical model predictions of H_{cr} (solid lines in Fig. 13(a)) are obtained by integrating the mathematical model introduced by the authors, for different values of S , and by assuming the geometrical and mechanical properties listed in Fig. 13(a). This is possible because, depending on the solver and timestep set, the mathematical model takes a few seconds to run. Each point in Fig. 13(a) corresponds to the first H (non-nil) value for which condition $U_{t,diff} = 0$ is satisfied (point P in Figs 13(a) and 13(b) corresponds to $S = 3$). For completeness, both BS 8006-1 (BSI, 2010)-ASIRI (2012) and McGuire (2011) are plotted in Fig. 13(b) as dashed vertical lines. For $S = 3$, BS 8006-1 (BSI, 2010) and ASIRI (2012) provide an unsafe estimation of the

critical height if compared to both McGuire (2011) and the mathematical model proposed herein.

CONCLUSIONS

In this paper, a new mathematical model is presented, for rapidly assessing the evolution with time of both average and differential settlements induced by static loads at the top of pile supported embankments founded on saturated soft soil layers. The mathematical model is representative for the embankment central zone, since it has been conceived for reproducing the mechanical response of an axisymmetric unit cell. It derives from the substructuring of the spatial domain and is based on the concepts of PES, arching and process zone. The employed sub-structuring scheme is very versatile and suitable to be extended to the case of geosynthetic reinforced embankments, rough and floating piles.

The mathematical model offers an improved understanding of the mechanical response of piled embankments. The model is also suitable for evaluating the critical height of the embankment, which was found to be dependent on the relative stiffness of the embankment with respect to stiffness of the foundation soil and on the embankment construction rate.

The novelty of this paper concerns the study of stress-transfer mechanisms from the embankment to the piles, in case of fine-grained soils in the foundation, demonstrating that these are severely influenced by the temporal evolution of pore pressure in the subsoil. In case of embankment constructed under drained conditions, geometrical non-linearities, due to the evolution of the embankment height, influence the evolution of the position of the PES. In contrast, in case of fine-grained subsoils, the construction phase mainly takes place under undrained conditions in the central region of the embankment, without inducing the activation of stress-transfer mechanisms from the embankment to piles. The PES starts evolving, at constant geometry, only when consolidation takes place and, in general, after the embankment construction.

The hypotheses introduced to obtain the FE numerical results, from which the mathematical model is derived, are particularly restrictive (axisymmetric conditions, smooth shaft piles and embankment construction under undrained conditions). For this reason, in addition to validation against

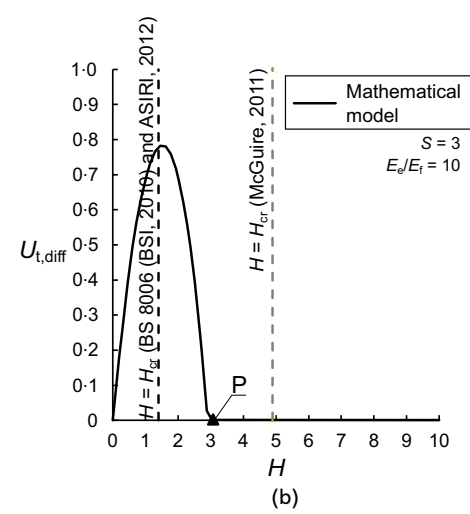
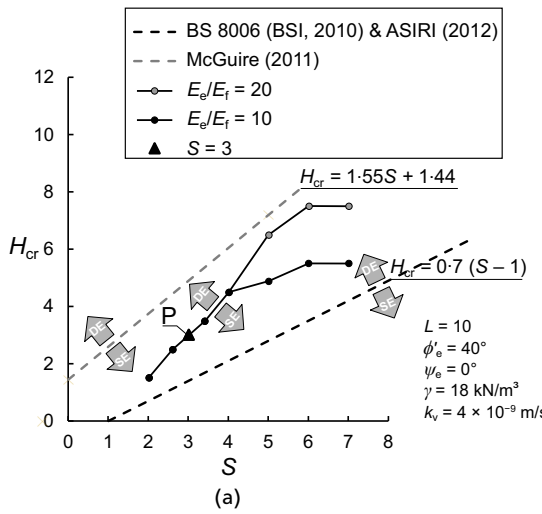


Fig. 13. (a) Critical height as a function of pile spacing for BS 8006 (BSI, 2010), ASIRI (2012), McGuire (2011) and the mathematical model, at the long term for different E_e/E_f ratios. (b) Estimation of critical height for $S = 3$ using the mathematical model: long-term differential settlements at the top of the embankment against different values of embankment final height

a numerical parametric study, the authors employed some experimental data and other numerical analyses taken from the literature to further validate the mathematical model, without pretending to reproduce the measurements perfectly.

The mathematical model allows, once geometry and mechanical properties are assigned, a very rapid estimation of the system performance. In the pre-design stage, once (a) thickness of both embankment and soft soil stratum and (b) their mechanical properties are known, the mathematical model may be employed as a tool to optimise both diameter and pile spacing.

DATA AVAILABILITY STATEMENT

Some or all data, models or code that support the findings of this study are available from the corresponding author upon reasonable request.

$$C_{\text{diff}}(\chi, H) = \begin{cases} 0 & \text{if } \mathcal{T}_e < \mathcal{T}_{ey} \\ \frac{S^2 \bar{k} \tan \phi'_{ss} E_{\text{oed},f}}{3L(S^2 - 1)E_{\text{oed},e}} \left\{ F_{31}^{\text{ep}} [2H_{ey}(H_{ey} + 2H_p - 2H) + 3H_p(3H_p - 8H)] - 4(H_{ey}H_p + H_{ey}^2 + 3H_p^2) \right\} & \text{if } \mathcal{T}_e = \mathcal{T}_{ey} \end{cases} \quad (38)$$

$$\Phi_{\text{diff}}(\chi, H) = \begin{cases} 0 & \text{if } \mathcal{T}_e < \mathcal{T}_{ey} \\ \frac{\mathcal{U}_w}{\eta} - \frac{S^2 \bar{k} \tan \phi'_{ss} E_{\text{oed},f}}{3L(S^2 - 1)E_{\text{oed},e}} [2(2H - 2H_p - H_{ey})H_{ey} + 3(8H - 3H_p)H_p] F_{32}^{\text{ep}} & \text{if } \mathcal{T}_e = \mathcal{T}_{ey} \end{cases} \quad (39)$$

NOTATION

$C_{2, 3, \dots, 8}$	non-dimensional compliance of subdomains defined in the model
$C_{\text{av}}, C_{\text{diff}}$	non-dimensional compliances of the model
C_e	generalised non-dimensional elastic compliance for I_e interface element
d	pile diameter (m)
E_e, E_f	Young's modulus of embankment and foundation soil, respectively (kPa)
$E_{\text{oed},e}, E_{\text{oed},f}$	oedometric modulus of embankment and foundation soil, respectively (kPa)
$\mathbf{F}^e, \mathbf{F}^{\text{ep}}$	matrix of terms defining the hidden non-dimensional variables during the elastic and elastic-plastic phase, respectively
H	non-dimensional embankment height
H_{cr}	non-dimensional critical embankment height
H_e	non-dimensional height subdomains 5–6
H_{ey}	constant value of H_e after yielding
H_p	non-dimensional process height
H^*	non-dimensional distance of the plane of equal settlements (PES) from the embankment bottom
h	embankment height (m)
h_{cr}	critical embankment height (i.e. h^* at the end of consolidation) (m)
h_e	height of the elastic zone in the embankment (m)
h_p	process height of the embankment (see subsection 'Process height') (m)
h^*	distance of the PES from the embankment bottom (m)
I_e, I_p	elastic and plastic interface elements in the model, respectively
k	ratio between horizontal and vertical stresses
\bar{k}	average value of the k ratio in the process zone
k_v	vertical hydraulic conductivity of the foundation soil (m/s)
L	non-dimensional pile length
l	pile length (m)
r	radial coordinate (m)
S	non-dimensional unit cell diameter

ACKNOWLEDGEMENTS

The authors acknowledge Professor Laurent Briançon for his willingness to share important information about the full-scale test. Professor J. Dijkstra and Dr V. Mangraviti gratefully acknowledge the support of the NordForsk project #98335 NordicLink.

Appendix

$$C_{\text{av}}(H) = \frac{E_{\text{oed},f}}{E_{\text{oed},e}} \frac{H}{L} \quad (36)$$

$$\Phi_{\text{av}}(\chi, H) = \frac{S^2 - 1}{S^2} \frac{\mathcal{U}_w}{\eta} \quad (37)$$

$$0 \text{ if } \mathcal{T}_e < \mathcal{T}_{ey}$$

s	unit cell diameter (m)
T	non-dimensional time
\mathcal{T}_e	non-dimensional shear force transferred by I_e
\mathcal{T}_{ey}	non-dimensional \mathcal{T}_e at yielding
\mathcal{T}_p	non-dimensional shear force transferred by I_p
t	time (s)
t_y	yielding time (s)
$U_{b,f}$	non-dimensional $u_{b,f}$
$U_{e,c}$	non-dimensional average settlement of the top of subdomain 5
$U_{e,\text{diff}}$	non-dimensional (nil) differential settlement at PES
$U_{e,f}$	non-dimensional average settlement of the top of subdomain 6
$U_{t,\text{av}}$	non-dimensional $u_{t,\text{av}}$
$U_{t,\text{diff}}$	non-dimensional $u_{t,\text{diff}}$
U_w	non-dimensional average stresses acting on the dashpot of subdomain 2
u_b	vertical displacement at the base of the embankment ($z = 0$) (m)
$u_{b,f}$	average settlement of the base of the embankment (m)
u_t	vertical displacement at the top of the embankment ($z = h$) (m)
$u_{t,\text{av}}$	average settlement at the top of the embankment (m)
$u_{t,c}$	average displacement of the top of the embankment for $0 < r < d/2$ (m)
$u_{t,\text{diff}}$	dimensional differential settlement at the top of the embankment (m)
$u_{t,f}$	average displacement of the top of the embankment for $d/2 < r < s/2$ (m)
Z	non-dimensional z
z	vertical coordinate (m)
γ	unit weight of embankment (kN/m^3)
γ_w	water unit weight (kN/m^3)
η	non-dimensional viscosity of the dashpot of subdomain 2
Σ_c	non-dimensional σ_c
Σ_f	non-dimensional σ_f

Σ'_f	non-dimensional average vertical stress at the top of subdomain 2 at the end of consolidation	roughness. <i>Eur. J. Environ. Civ. Engng</i> 27 , No. 1, 194–214, https://doi.org/10.1080/19648189.2022.2035259 .
σ_c	average total vertical stress acting above the concrete pile (kPa)	Girout, R., Blanc, M., Thorel, L., Fagundes, D. F. & Almeida, M. S. S. (2016). Arching and deformation in a piled embankment: centrifuge tests compared to analytical calculations. <i>J. Geotech. Geoenviron. Engng</i> 142 , No. 12, 04016069, https://doi.org/10.1061/(ASCE)GT.1943-5606.0001557 .
σ_f	average total vertical stress acting above the foundation soil (kPa)	Han, J. & Akins, K. (2002). Use of geogrid-reinforced and pile-supported earth structures. <i>Deep foundations 2002, Proceedings</i> , https://doi.org/10.1061/40601(256)48 .
σ_v	total vertical stress at the base of the embankment (kPa)	Han, J., Oztoprak, S., Parsons, R. L. & Huang, J. (2007). Numerical analysis of foundation columns to support widening of embankments. <i>Comput. Geotech.</i> 34 , No. 6, 435–448, https://doi.org/10.1016/j.compgeo.2007.01.006 .
τ_0	maximum shear stress within the elastic zone (kPa)	Huang, J. & Han, J. (2010). Two-dimensional parametric study of geosynthetic-reinforced column-supported embankments by coupled hydraulic and mechanical modeling. <i>Comput. Geotech.</i> 37 , No. 5, 638–648, https://doi.org/10.1016/j.compgeo.2010.04.002 .
τ_{pl}	shear stress at yielding in $z = 0$ (kPa)	Iglesia, G. R., Einstein, H. H. & Whitman, R. V. (2014). Investigation of soil arching with centrifuge tests. <i>J. Geotech. Geoenviron. Engng</i> 140 , No. 2, 04013005, https://doi.org/10.1061/(ASCE)GT.1943-5606.0000998 .
Φ_{av}, Φ_{diff}	non-dimensional settlements rate during consolidation	Jenck, O., Dias, D. & Kastner, R. (2007). Two-dimensional physical and numerical modeling of a pile-supported earth platform over soft soil. <i>J. Geotech. Geoenviron. Engng</i> 133 , No. 3, 295–305, https://doi.org/10.1061/(asce)1090-0241(2007)133:3(295) .
ϕ'_e	embankment soil internal friction angle (degrees)	Jenck, O., Dias, D. & Kastner, R. (2009). Three-dimensional numerical modeling of a piled embankment. <i>Int. J. Geomech.</i> 9 , No. 3, 102–112, https://doi.org/10.1061/(asce)1532-3641(2009)9:3(102) .
ϕ'_{ss}	embankment soil simple shear friction angle (degrees)	King, D. J., Bouazza, A., Gniel, J. R., Rowe, R. K. & Bui, H. H. (2017). Load-transfer platform behaviour in embankments supported on semi-rigid columns: implications of the ground reaction curve. <i>Can. Geotech. J.</i> 54 , No. 8, 1158–1175, https://doi.org/10.1139/cjg-2016-0406 .
χ	vector of hidden non-dimensional variables	King, L., Bouazza, A., Dubsky, S., Rowe, R. K., Gniel, J. & Bui, H. H. (2019). Kinematics of soil arching in piled embankments. <i>Géotechnique</i> 69 , No. 11, 941–958, https://doi.org/10.1680/jgeot.18.P.104 .
ψ_e	embankment soil dilatancy angle (degrees)	Liu, H., Luo, Q., Naggar, M. H., El Asce, F., Zhang, L. & Wang, T. (2023). Centrifuge modeling of stability of embankment on soft soil improved by rigid columns. <i>J. Geotech. Geoenviron. Engng</i> 149 , No. 9, 1–15, https://doi.org/10.1061/JGGEFK.GTENG-11314 .
Σ'_f	non-dimensional average vertical stress at the top of subdomain 2 at the end of consolidation	roughness. <i>Eur. J. Environ. Civ. Engng</i> 27 , No. 1, 194–214, https://doi.org/10.1080/19648189.2022.2035259 .
σ_c	average total vertical stress acting above the concrete pile (kPa)	Girout, R., Blanc, M., Thorel, L., Fagundes, D. F. & Almeida, M. S. S. (2016). Arching and deformation in a piled embankment: centrifuge tests compared to analytical calculations. <i>J. Geotech. Geoenviron. Engng</i> 142 , No. 12, 04016069, https://doi.org/10.1061/(ASCE)GT.1943-5606.0001557 .
σ_f	average total vertical stress acting above the foundation soil (kPa)	Han, J. & Akins, K. (2002). Use of geogrid-reinforced and pile-supported earth structures. <i>Deep foundations 2002, Proceedings</i> , https://doi.org/10.1061/40601(256)48 .
σ_v	total vertical stress at the base of the embankment (kPa)	Han, J., Oztoprak, S., Parsons, R. L. & Huang, J. (2007). Numerical analysis of foundation columns to support widening of embankments. <i>Comput. Geotech.</i> 34 , No. 6, 435–448, https://doi.org/10.1016/j.compgeo.2007.01.006 .
τ_0	maximum shear stress within the elastic zone (kPa)	Huang, J. & Han, J. (2010). Two-dimensional parametric study of geosynthetic-reinforced column-supported embankments by coupled hydraulic and mechanical modeling. <i>Comput. Geotech.</i> 37 , No. 5, 638–648, https://doi.org/10.1016/j.compgeo.2010.04.002 .
τ_{pl}	shear stress at yielding in $z = 0$ (kPa)	Iglesia, G. R., Einstein, H. H. & Whitman, R. V. (2014). Investigation of soil arching with centrifuge tests. <i>J. Geotech. Geoenviron. Engng</i> 140 , No. 2, 04013005, https://doi.org/10.1061/(ASCE)GT.1943-5606.0000998 .
Φ_{av}, Φ_{diff}	non-dimensional settlements rate during consolidation	Jenck, O., Dias, D. & Kastner, R. (2007). Two-dimensional physical and numerical modeling of a pile-supported earth platform over soft soil. <i>J. Geotech. Geoenviron. Engng</i> 133 , No. 3, 295–305, https://doi.org/10.1061/(asce)1090-0241(2007)133:3(295) .
ϕ'_e	embankment soil internal friction angle (degrees)	Jenck, O., Dias, D. & Kastner, R. (2009). Three-dimensional numerical modeling of a piled embankment. <i>Int. J. Geomech.</i> 9 , No. 3, 102–112, https://doi.org/10.1061/(asce)1532-3641(2009)9:3(102) .
ϕ'_{ss}	embankment soil simple shear friction angle (degrees)	King, D. J., Bouazza, A., Gniel, J. R., Rowe, R. K. & Bui, H. H. (2017). Load-transfer platform behaviour in embankments supported on semi-rigid columns: implications of the ground reaction curve. <i>Can. Geotech. J.</i> 54 , No. 8, 1158–1175, https://doi.org/10.1139/cjg-2016-0406 .
χ	vector of hidden non-dimensional variables	King, L., Bouazza, A., Dubsky, S., Rowe, R. K., Gniel, J. & Bui, H. H. (2019). Kinematics of soil arching in piled embankments. <i>Géotechnique</i> 69 , No. 11, 941–958, https://doi.org/10.1680/jgeot.18.P.104 .
ψ_e	embankment soil dilatancy angle (degrees)	Liu, H., Luo, Q., Naggar, M. H., El Asce, F., Zhang, L. & Wang, T. (2023). Centrifuge modeling of stability of embankment on soft soil improved by rigid columns. <i>J. Geotech. Geoenviron. Engng</i> 149 , No. 9, 1–15, https://doi.org/10.1061/JGGEFK.GTENG-11314 .

REFERENCES

ASIRI (2012) Recommendations for the design, construction and control of rigid: Inclusion ground improvements. ASIRI National Project.

Bhasi, A. & Rajagopal, K. (2015). Geosynthetic-reinforced piled embankments: comparison of numerical and analytical methods. *Int. J. Geomech.* **15**, No. 5, 04014074, [https://doi.org/10.1061/\(asce\)gm.1943-5622.0000414](https://doi.org/10.1061/(asce)gm.1943-5622.0000414).

Briançon, L. & Simon, B. (2012). Performance of pile-supported embankment over soft soil: full-scale experiment. *J. Geotech. Geoenviron. Engng* **138**, No. 4, 551–561, [https://doi.org/10.1061/\(ASCE\)GT.1943-5606.0000561](https://doi.org/10.1061/(ASCE)GT.1943-5606.0000561).

BSI (2010). BS 8006-1: Code of practice for strengthened/reinforced soils and other fills. London, UK: BSI.

Chen, R. P., Chen, Y. M., Han, J. & Xu, Z. Z. (2008). A theoretical solution for pile-supported embankments on soft soils under one-dimensional compression. *Can. Geotech. J.* **45**, No. 5, 611–623, <https://doi.org/10.1139/T08-003>.

Combarieu, O. (1988). Amelioration of soils by vertical rigid piles application to construction of embankments on soft soils. *Rev. Fr. Geotech.* No. 44, 57–79 (in French).

Cuira, F. & Simon, B. (2009). Deux outils simples pour traiter des interactions complexes d'un massif renforcé par inclusions rigides two simple tools for evaluating the complex interactions in a soil reinforced by rigid inclusions. In *17th ICSMGE*. Alexandria, <https://doi.org/10.3233/978-1-60750-031-5-1550> (in French).

Da Silva Burke, T. S. & Elshafie, M. Z. E. B. (2021). Arching in granular soils: experimental observations of deformation mechanisms. *Géotechnique* **71**, No. 10, 866–878, <https://doi.org/10.1680/jgeot.19.P.174>.

di Prisco, C., Flessati, L., Galli, A. & Mangraviti, V. (2019). A simplified approach for the estimation of settlements of earth embankments on piled foundations. In *Lecture notes in civil engineering* (eds F. Calvetti, F. Cotecchia, A. Galli & C. Jommi), pp. 640–648. Cham, Switzerland: Springer International Publishing, https://doi.org/10.1007/978-3-030-21359-6_68.

di Prisco, C., Flessati, L., Frigerio, G. & Galli, A. (2020). Mathematical modelling of the mechanical response of earth embankments on piled foundations. *Géotechnique* **70**, No. 9, 755–773, <https://doi.org/10.1680/jgeot.18.P.127>.

EBGEO (2010). *Empfehlungen für den Entwurf und die Berechnung von Erdkörpern mit Bewehrungen aus Geokunststoffen – EBGEO*. Weinheim, Germany: Wiley-VCH Verlag GmbH & Co. KGaA, <https://doi.org/10.1002/9783433600597> (in German).

Feng, S., Xu, R., Yu, J., Zhang, C. & Cheng, K. (2021). Field monitoring of geogrid-reinforced and pile-supported embankment at bridge approach. *Int. J. Geosynth. Ground Engng* **7**, No. 1, <https://doi.org/10.1007/s40891-020-00248-5>.

Flessati, L., di Prisco, C., Corigliano, M. & Mangraviti, V. (2023). A simplified approach to estimate settlements of earth embankments on piled foundations: the role of pile shaft roughness. *Eur. J. Environ. Civ. Engng* **27**, No. 1, 194–214, <https://doi.org/10.1080/19648189.2022.2035259>.

Girout, R., Blanc, M., Thorel, L., Fagundes, D. F. & Almeida, M. S. S. (2016). Arching and deformation in a piled embankment: centrifuge tests compared to analytical calculations. *J. Geotech. Geoenviron. Engng* **142**, No. 12, 04016069, [https://doi.org/10.1061/\(ASCE\)GT.1943-5606.0001557](https://doi.org/10.1061/(ASCE)GT.1943-5606.0001557).

Han, J. & Akins, K. (2002). Use of geogrid-reinforced and pile-supported earth structures. *Deep foundations 2002, Proceedings*, [https://doi.org/10.1061/40601\(256\)48](https://doi.org/10.1061/40601(256)48).

Han, J., Oztoprak, S., Parsons, R. L. & Huang, J. (2007). Numerical analysis of foundation columns to support widening of embankments. *Comput. Geotech.* **34**, No. 6, 435–448, <https://doi.org/10.1016/j.compgeo.2007.01.006>.

Huang, J. & Han, J. (2010). Two-dimensional parametric study of geosynthetic-reinforced column-supported embankments by coupled hydraulic and mechanical modeling. *Comput. Geotech.* **37**, No. 5, 638–648, <https://doi.org/10.1016/j.compgeo.2010.04.002>.

Iglesia, G. R., Einstein, H. H. & Whitman, R. V. (2014). Investigation of soil arching with centrifuge tests. *J. Geotech. Geoenviron. Engng* **140**, No. 2, 04013005, [https://doi.org/10.1061/\(ASCE\)GT.1943-5606.0000998](https://doi.org/10.1061/(ASCE)GT.1943-5606.0000998).

Jenck, O., Dias, D. & Kastner, R. (2007). Two-dimensional physical and numerical modeling of a pile-supported earth platform over soft soil. *J. Geotech. Geoenviron. Engng* **133**, No. 3, 295–305, [https://doi.org/10.1061/\(asce\)1090-0241\(2007\)133:3\(295\)](https://doi.org/10.1061/(asce)1090-0241(2007)133:3(295)).

Jenck, O., Dias, D. & Kastner, R. (2009). Three-dimensional numerical modeling of a piled embankment. *Int. J. Geomech.* **9**, No. 3, 102–112, [https://doi.org/10.1061/\(asce\)1532-3641\(2009\)9:3\(102\)](https://doi.org/10.1061/(asce)1532-3641(2009)9:3(102)).

King, D. J., Bouazza, A., Gniel, J. R., Rowe, R. K. & Bui, H. H. (2017). Load-transfer platform behaviour in embankments supported on semi-rigid columns: implications of the ground reaction curve. *Can. Geotech. J.* **54**, No. 8, 1158–1175, <https://doi.org/10.1139/cjg-2016-0406>.

King, L., Bouazza, A., Dubsky, S., Rowe, R. K., Gniel, J. & Bui, H. H. (2019). Kinematics of soil arching in piled embankments. *Géotechnique* **69**, No. 11, 941–958, <https://doi.org/10.1680/jgeot.18.P.104>.

Liu, H., Luo, Q., Naggar, M. H., El Asce, F., Zhang, L. & Wang, T. (2023). Centrifuge modeling of stability of embankment on soft soil improved by rigid columns. *J. Geotech. Geoenviron. Engng* **149**, No. 9, 1–15, <https://doi.org/10.1061/JGGEFK.GTENG-11314>.

Lu, W., Miao, L., Wang, F., Zhang, J., Zhang, Y. & Wang, H. (2020). A case study on geogrid-reinforced and pile-supported widened highway embankment. *Geosynth. Int.* **27**, No. 3, 261–274, <https://doi.org/10.1680/jgein.19.00024>.

Lu, W. H., Miao, L. C., Wang, F., Cai, H. S. & Zhang, C. X. (2013). Experimental study of soil arching of geogrid-reinforced and pile-supported widening embankment. *Yantu Lixuel/Rock Soil Mech.* **34**, No. 8, 2316–2322.

Mangraviti, V. (2021). *Theoretical modelling of embankments based on piled foundations*. PhD thesis, Politecnico di Milano.

Mangraviti, V. (2022). Displacement-based design of geosynthetic-reinforced pile-supported embankments to increase sustainability. In *Civil and environmental engineering for the sustainable development goals: Emerging issues* (eds M. Antonelli and G. Della Vecchia), pp. 83–96. Cham, Switzerland: Springer International Publishing, https://doi.org/10.1007/978-3-030-99593-5_7.

Mangraviti, V., Flessati, L. & di Prisco, C. (2021). Modelling the development of settlements of earth embankments on piled foundations. In *Lecture notes in civil engineering* (eds M. Barla, A. Di Donna and D. Sterpi), pp. 811–816. Cham, Switzerland: Springer International Publishing, https://doi.org/10.1007/978-3-030-64518-2_96.

Mangraviti, V., Flessati, L. & di Prisco, C. (2023a). Geosynthetic-reinforced and pile-supported embankments: theoretical discussion of finite difference numerical analyses results. *Eur. J. Environ. Civ. Engng* **27**, No. 15, 4337–4363, <https://doi.org/10.1080/19648189.2023.2190400>.

Mangraviti, V., Flessati, L. & di Prisco, C. (2023b). Mathematical modelling of the mechanical response of

geosynthetic-reinforced and pile-supported embankments. *Numer. Analyt. Methods Geomech.* **47**, No. 13, 2438–2466, <https://doi.org/10.1002/nag.3586>.

Marston, A. (1913). The theory of loads on pipe in ditches and tests of cement and clay drain tile and sewer pipe. Iowa State College of Agriculture and Mechanic Arts.

Matlab (2022) MATLAB version: 9.13.0 (R2022b), Natick, Massachusetts: The MathWorks Inc. See <https://www.mathworks.com>.

McGuire, M. P. (2011). Critical height and surface deformation of column-supported embankments. Virginia Polytechnic Institute and State University.

McKelvey, J. A. (1994). The anatomy of soil arching. *Geotext. Geomembr.* **13**, No. 5, 317–329, [https://doi.org/10.1016/0266-1144\(94\)90026-4](https://doi.org/10.1016/0266-1144(94)90026-4).

Naughton, P. J. & Kempton, G. T. (2005). Comparison of analytical and numerical analysis design methods for piled embankments. In *GeoFrontiers 2005: Contemporary issues in foundation engineering* (eds J. B. Anderson, K. K. Phoon, E. Smith and J. E. Loehr). Reston, VA, USA: American Society of Civil Engineers, [https://doi.org/10.1061/40777\(156\)11](https://doi.org/10.1061/40777(156)11).

Nunez, M. A., Briançon, L. & Dias, D. (2013). Analyses of a pile-supported embankment over soft clay: full-scale experiment, analytical and numerical approaches. *Engng Geol.* **153**, 53–67, <https://doi.org/10.1016/j.enggeo.2012.11.006>.

Oh, Y. I. & Shin, E. C. (2007). Reinforcement and arching effect of geogrid-reinforced and pile-supported embankment on marine soft ground. *Mar. Georesour. Geotechnol.* **25**, No. 2, 97–118, <https://doi.org/10.1080/10641190701359591>.

Okyay, U. S., Dias, D., Thorel, L. & Rault, G. (2014). Centrifuge modeling of a pile-supported granular earth-platform. *J. Geotech. Geoenviron. Engng* **140**, No. 2, [https://doi.org/10.1061/\(asce\)gt.1943-5606.0001004](https://doi.org/10.1061/(asce)gt.1943-5606.0001004).

Pham, T. A. & Dias, D. (2021). Comparison and evaluation of analytical models for the design of geosynthetic-reinforced and pile-supported embankments. *Geotext. Geomembr.* **49**, No. 3, 528–549, <https://doi.org/10.1016/j.geotexmem.2020.11.001>.

Rowe, R. K. & Liu, K. W. (2015). Three-dimensional finite element modelling of a full-scale geosynthetic-reinforced, pile-supported embankment. *Can. Geotech. J.* **52**, No. 12, 2041–2054, <https://doi.org/10.1139/cgj-2014-0506>.

Smith, M. & Filz, G. (2007). Axisymmetric numerical modeling of a unit cell in geosynthetic-reinforced, column-supported embankments. *Geosynth. Int.* **14**, No. 1, 13–22, <https://doi.org/10.1680/gein.2007.14.1.13>.

Terzaghi, K. (1936). Stress distribution in dry and in saturated sand above a yielding trap-door. International Society for Soil Mechanics and Geotechnical Engineering, pp. 536–537.

See <https://www.issmge.org/publications/publication/stress-distribution-in-dry-and-in-saturated-sand-above-a-yielding-trap-door>.

Tochnog Professional (2019). *Tochnog Professional, Version 22*. See www.tochnogprofessional.nl (accessed 02/05/2025).

Van Duijnen, P. G., Van Eekelen, S. J. M. & Van Der Stoel, A. E. C. (2010). Monitoring of a railway piled embankment. *9th international conference on geosynthetics – Geosynthetics: advanced solutions for a challenging world, ICG 2010*, pp. 1461–1464.

van Eekelen S. J. M. & Brugman M. H. A. (eds) (2016). *Design guideline basal reinforced piled embankments*, CUR226. The Netherlands: SBRCURnet/Boca Raton, FL, USA: CRC Press.

Van Eekelen, S. J. M., Bezuijen, A. & Alexiew, D. (2010). The Kyoto road piled embankment: 31/2 years of measurements. *9th international conference on geosynthetics – Geosynthetics: advanced solutions for a challenging world, ICG 2010*, Guaruja, Brazil, pp. 1941–1944.

van Eekelen, S. J. M., Bezuijen, A., Lodder, H. J. & van Tol, A. F. (2012). Model experiments on piled embankments. Part II. *Geotext. Geomembr.* **32**, 82–94, <https://doi.org/10.1016/j.geotexmem.2011.11.003>.

van Eekelen, S. J. M., Bezuijen, A. & van Tol, A. F. (2013). An analytical model for arching in piled embankments. *Geotext. Geomembr.* **39**, 78–102, <https://doi.org/10.1016/j.geotexmem.2013.07.005>.

van Eekelen, S. J. M., Venmans, A. A. M., Bezuijen, A. & van Tol, A. F. (2020). Long term measurements in the Woerden geosynthetic-reinforced pile-supported embankment. *Geosynth. Int.* **27**, No. 2, 142–156, <https://doi.org/10.1680/jgein.17.00022>.

Wijerathna, M. & Liyanapathirana, D. S. (2020). Load transfer mechanism in geosynthetic reinforced column-supported embankments. *Geosynth. Int.* **27**, No. 3, 236–248, <https://doi.org/10.1680/jgein.19.00022>.

Xing, H., Zhang, Z., Liu, H. & Wei, H. (2014). Large-scale tests of pile-supported earth platform with and without geogrid. *Geotext. Geomembr.* **42**, No. 6, 586–598, <https://doi.org/10.1016/j.geotexmem.2014.10.005>.

Yu, J. L., Zhou, J. J., Gong, X. N., Xu, R. Q., Li, J. Y. & Xu, S. D. (2021). Centrifuge study on behavior of rigid pile composite foundation under embankment in soft soil. *Acta Geotech.* **16**, No. 6, 1909–1921, <https://doi.org/10.1007/s11440-020-01109-1>.

Zheng, G., Yang, X., Zhou, H. & Chai, J. (2019). Numerical modeling of progressive failure of rigid piles under embankment load. *Can. Geotech. J.* **56**, No. 1, 23–34, <https://doi.org/10.1139/cgj-2017-0613>.